Practical Fidelity Limits of Toffoli Gates in Superconducting Quantum Processors

M. AbuGhanem^{1,2}

 Faculty of Science, Ain Shams University, Cairo, 11566, Egypt and
 Zewail City of Science, Technology and Innovation, Giza, 12678, Egypt* (Dated: May 9, 2025)

High-fidelity multi-qubit gates are a critical resource for near-term quantum computing, as they underpin the execution of both quantum algorithms and fault-tolerant protocols. The Toffoli gate (CCNOT), in particular, plays a central role in quantum error correction and quantum arithmetic, yet its efficient implementation on current quantum hardware remains limited by noise and connectivity constraints. In this work, we present a hardware-aware characterization of the Toffoli gate using optimized, connectivity-compliant decompositions executed on IBM's 127-qubit superconducting quantum processors. Our study integrates state preparation, gate synthesis, and quantum state/process tomography (QST/QPT) to evaluate fidelity across three distinct classes of input states: Greenberger-Horne-Zeilinger (GHZ), W, and the uniform superposition of all three-qubit computational basis states—under noise-free simulation, noise-aware emulation, and real hardware execution. For GHZ states, we report state fidelities of 98.442% (noise-free simulation), 81.470% (noise-aware quantum emulation), and 56.368% (real quantum hardware). For W states, state fidelities are 98.739%, 79.900%, and 63.689%, respectively, and for the uniform superposition state, we observe state fidelities of 99.490%, 85.469%, and 61.161%. Comparative QPT experiments yield process fidelities of 98.976% (noise-free) and 80.160% (noise-aware emulation). Our results empirically characterize state-dependent error patterns in multi-qubit circuits and quantify trade-offs between gate decomposition strategies and native hardware performance, offering practical insights for scalable, hardware-efficient quantum circuit design.

Keywords: Toffoli gate, superconducting quantum processors, state-dependent error patterns, quantum state tomography, quantum process tomography, NISQ era, Greenberger–Horne–Zeilinger, IBM's quantum computers, error characterization.

PACS: 03.67.Lx, 03.67.-a, 03.67.Ac

I. INTRODUCTION

Quantum computers [1, 2] harness the principles of quantum superposition and entanglement [3, 4] to solve problems intractable for classical systems [5–12], from simulating quantum materials [13] and drug design [14, 15] to advancing global supply chains [16] and accelerating cryptographic breakthroughs [17, 18]. Quantum computers holds immense promise for real-world applications [2], enabling industries to tackle complex challenges with unprecedented efficiency, accuracy, and cost-effectiveness [2, 19]. While fault-tolerant architectures—systems capable of maintaining computational accuracy despite inherent noise, decoherence, and hardware imperfections—promise transformative applications [20, 21]. Today's noisy intermediate-scale quantum (NISQ) processors [10] face stringent limitations in qubit count, coherence times, and gate fidelity [22]. Realizing practical advantages on these systems demands efficient implementations of fundamental operations—particularly multi-qubit gates that encode conditional logic [23].

Among these, the Toffoli gate [24] stands as a cornerstone of quantum computation, enabling universal classical and quantum logic when combined with single-qubit operations [25]. Its ability to perform controlled operations on three qubits makes it indispensable for quantum algorithms ranging from error correction [20, 21] to arithmetic circuits [26]. However, implementing high-fidelity Toffoli gates on NISQ processors remains a challenge, as the gate's complexity exacerbates the effects of decoherence, crosstalk, and calibration errors [22].

While superconducting quantum processors [27] have demonstrated remarkable progress in one- and two-qubit gate fidelities [9–11, 28], three-qubit gates like the Toffoli gate [24] often require decomposition into native gates, introducing additional overhead and noise [29, 30]. Recent work has explored both direct implementations [25, 31] and optimized decompositions (as discussed in Section II), but a systematic characterization of the gate's performance across different input states—particularly entangled states relevant to algorithms—is still lacking.

In this work, we present a comprehensive experimental study of the Toffoli gate [24] performance on state-of-the-art superconducting processors from IBM Quantum ($ibm_sherbrooke$ and $ibm_brisbane$) [2]. To understanding their behavior across diverse input states on real hardware, using full quantum state tomography, we evaluate the gate's state fidelity for three critical input states: Greenberger–Horne–Zeilinger (GHZ) states (($|000\rangle + |111\rangle$)/ $\sqrt{2}$), testing coherence in maximally entangled systems; W states (($|001\rangle + |010\rangle + |100\rangle$)/ $\sqrt{3}$), sensitive to asymmetric errors; Uniform superpositions ($\sum_{x \in \{0,1\}^3} |x\rangle/\sqrt{8}$), probing basis-state-independent behavior

Quantum tomography provides a powerful lens to evaluate gate performance beyond average fidelity metrics.

^{*} gaa1nem@gmail.com

QST reconstructs the output density matrix, revealing how specific input states degrade under noise [32]. Meanwhile, QPT fully characterizes the gate's operation, identifying dominant error channels [33, 34]. These tools are essential for debugging and optimizing gates in practice [35–38].

We complement these measurements with a full QPT analysis of the Toffoli gate [24] on both noiseless quantum simulator and noisy quantum emulator; by employing a comprehensive tomography framework that combines quantum QST and QPT to evaluate gate performance in three key regimes. First, we assess entanglement resilience using GHZ and W states, which serve as stringent tests of coherence under maximal entanglement conditions. Second, we examine basis-state uniformity through uniform superposition states, revealing systematic biases in the computational basis. Finally, by comparing real quantum hardware results with both noiseless quantum simulator and noisy quantum emulator benchmarks, we precisely quantify noise-induced deviations in gate operation. Our results help bridge the gap between theoretical gate specifications and real-world implementation fidelity by providing detailed benchmarks for threequbit operations in NISQ-era quantum computing. The state-dependent error profiles and simulator-to-hardware comparisons we report provide a roadmap for optimizing three-qubit gates in NISQ-era quantum algorithms [39].

The remainder of this work is structured as follows: Section II reviews hardware-aware quantum circuit synthesis, with a focus on optimized Toffoli gate implementations for NISQ devices (Section II A). Section II C discusses hardware-specific decomposition techniques. Section III details our experimental setup, including: gate implementation protocols (Section III A), state preparation methodologies (Section III B), and quantum tomography procedures for fidelity validation (Section III C). Section IV analyzes results and discussion, comparing theoretical predictions with empirical data. Section V evaluates quantum hardware performance metrics across different superconducting quantum architectures. Lastly, Section VI concludes with key findings and future directions for scalable quantum circuit synthesis.

II. HARDWARE-AWARE QUANTUM CIRCUIT SYNTHESIS AND TOFFOLI GATE IMPLEMENTATIONS

A. Compilation Strategies for Robust Implementations

The optimization of quantum circuits is critical for enabling practical applications across dynamical simulations and combinatorial problem-solving. Current methodologies can be classified into several key approaches: problem-informed techniques that exploit dynamical symmetries [40–43], noise-resilient compilation strategies [44–47], hardware-adaptive gate set redefini-

tions [48], and numerical circuit synthesis leveraging computational search algorithms [49].

Recent advances in circuit synthesis have been propelled by enhanced computational resources and sophisticated optimization frameworks. These include discrete searches over finite gate sets [50, 51], hybrid discrete-continuous optimization [52, 53], adaptive synthesis protocols [54–57], and metaheuristic methods such as genetic algorithms [58, 59] and machine learning [60, 61]. Notably, emerging hybrid techniques [62, 63] integrate architectural search with continuous parameter optimization, building upon principles from variational compilation of random unitaries [49, 62]—a standard benchmark for assessing circuit complexity [64–66].

To execute high-level quantum algorithms on physical hardware, high-level circuit descriptions must be translated into device-specific native operations. This compilation process typically employs quantum assembly languages such as OpenQASM [67] as intermediate representations. Although quantum instruction sets fundamentally comprise 1-qubit rotations and 2-qubit CNOT gates, actual hardware implementations frequently demand additional decomposition into architecture-specific native gate sets. For instance, fixed-frequency superconducting quantum processors utilize the echoed cross-resonance (ECR) gate as their fundamental two-qubit operation [68].

The development of optimal gate decomposition methods represents a fundamental challenge in quantum compilation. Academic investigations have pursued two complementary directions: general techniques for arbitrary unitary operations [69–72] and specialized implementations for common quantum circuits, including Toffoli gates [73] and quantum Fourier transforms [74]. Modern approaches incorporate detailed hardware constraints into the compilation process, developing topology-aware decomposition methods that significantly reduce gate counts and circuit depth [75, 76].

Leading quantum compilation frameworks, including Qiskit [77], t|ket\ [78], and Cirq [79], implement sophisticated gate-level optimization pipelines. These systems incorporate multiple complementary techniques: redundant gate elimination through cancellation methods [80], optimal two-qubit gate synthesis via KAK decomposition [81], and adaptive circuit restructuring through dynamic gate reordering [82]. Compilers additionally employ specialized optimization strategies such as localized peephole circuit transformations [83], softwarebased crosstalk suppression [84], and noise resilience through dynamical decoupling sequences [85]. tionally, The QContext compiler [86], which pioneers a context-aware synthesis approach. This method simultaneously optimizes both abstract circuit representations and hardware-specific native gate implementations.

B. Multi-Qubit Toffoli Gates

As a paradigmatic multi-qubit operation, the Toffoli gate [24] represents a critical building block in quantum information processing, combining multiple control qubits with a single target qubit to enable conditional state manipulation [25]. First introduced by Tommaso Toffoli [24], this gate achieves computational universality when augmented with Hadamard operations [25, 87, 88], while simultaneously serving as a fundamental construct in reversible computing paradigms that connect classical and quantum computational models [89]. The gate's operational versatility is demonstrated through its essential role in cornerstone quantum algorithms including unstructured search (Grover's algorithm) [25, 90], prime factorization (Shor's algorithm) [91, 92], and faulttolerant circuit designs [93, 94], as well as various quantum error correction schemes [12, 95–97].

Formally, the k-qubit Toffoli gate family comprises k-1 control qubits governing the state inversion of a single target qubit, with the operation executing only when all control qubits occupy the $|1\rangle$ state [25]. The simplest non-trivial instance (k=2) reduces to the ubiquitous CNOT gate, while the 3-qubit variant (denoted as $\hat{\mathcal{V}}_{\text{Toffoli}}$) has emerged as particularly significant in quantum information theory.

This deceptively simple operation enables non-trivial computational power when combined with single-qubit gates, forming a universal gate set for quantum logic [28]. The underlying unitary transformation and quantum circuit representation for this three-qubit operation is given by:

Beyond its quantum applications, the Toffoli gate's classical simulation capability is noteworthy [24], as it can replicate any classical logic circuit while maintaining reversibility [24]. However, practical implementations face complexity barriers. Unlike native one- and two-qubit gates, three-qubit gates often require decomposition into lower-level operations—a process that introduces gate-depth overhead and amplifies errors [29]. For instance, typical implementations (assumes an ideal fully-connected quantum architecture) requiring decomposition into at least five 2-qubit gates [98] or six CNOT operations [25] when restricted to elementary 1- and 2-qubit gates [99]. These implementation challenges are further compounded in distributed quantum systems,

highlighting the intricate trade-offs between gate complexity and operational fidelity in physical realizations.

C. Hardware-Specific Decomposition Strategies

The Toffoli gate [24] has been implemented across various superconducting qubit architectures [27], with the canonical linear decomposition remaining one of the most widely used configurations [25]. However, practical deployment on NISQ devices is complicated by limited qubit connectivity, necessitating decompositions with minimal gate overhead. For instance, a three-qubit CCX gate typically requires at least six CNOT gates alongside single-qubit operations [25]. Typical decompositions use sequences of CNOT and single-qubit gates as depicted in Figure 1, but these may not align optimally with a processor's native gate set or connectivity.

Traditional decomposition methods often assume ideal, fully connected architectures—an unrealistic constraint for most of current quantum hardware. Alternative approaches, such as linear-topology-compatible decompositions using eight CNOT gates, have been explored [100] to address these limitations. A three-qubit CCX gate implementation requires 8 CNOT gates along with multiple single-qubit gates is depicted in Figure 2. Pulse-level optimizations have also been investigated [101], though these can introduce unintended SWAP operations between control qubits, which may not always be desirable.

Recent work by Bowman et al. [102] demonstrates hardware-conscious optimizations for the Toffoli gate [24] on IBM Quantum devices [2], reducing gate infidelity by 18% and cutting multi-qubit gate requirements through the use of multi-qubit cross-resonance gates [102]. Similarly, Cruz and Murta present shallow decompositions optimized for varying connectivity constraints, employing SWAP-efficient qubit reordering to minimize CNOT overhead [103].

Nemkov et al. introduce a variational synthesis method that co-optimizes architecture and parameters [49], achieving efficient decompositions for linear and star topologies. Ren et al. further advance hardware-aware circuit knitting by integrating gate cuts and SWAP insertions based on qubit interaction graphs [104]. Bennakhi et al. compare ancilla-based depth reduction techniques for multi-controlled X gates [105], highlighting the trade-offs between v-chain and recursive methods on NISQ hardware.

Wang et al. propose a hardware-efficient quantum random access memory implementation using native iSCZ, C-iSCZ gates, eliminating decomposition overhead while maintaining noise resilience [106]. Duckering et al.'s "Orchestrated Trios" approach [107] treats Toffoli gates as monolithic units during routing, deferring decomposition to post-mapping stages for improved CNOT efficiency. The study in [?] introduces a hardware-efficient ECR-based [109–112] Toffoli decomposition for superconducting architectures [2]. Experimental valida-

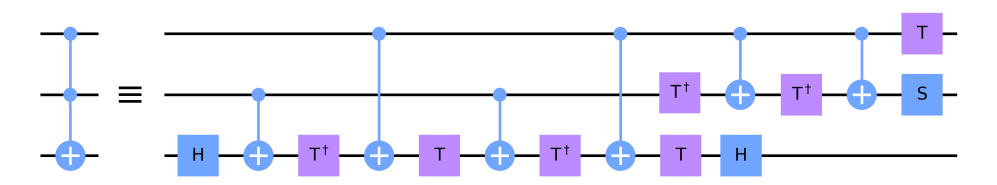


FIG. 1. A standard decomposition of a three-qubit CCX (Toffoli) gate requires six CNOT gates along with multiple single-qubit gates [25]. This conventional approach assumes an ideal fully-connected quantum architecture, a condition rarely met in NISQ-era devices due to their limited connectivity. This decomposition uses the following single-qubit gates: $H = \frac{1}{\sqrt{2}} \begin{pmatrix} 1 & 1 \\ 1 & -1 \end{pmatrix}$, $T = \begin{pmatrix} 1 & 0 \\ 0 & e^{i\pi/4} \end{pmatrix}$, $S = \begin{pmatrix} 1 & 0 \\ 0 & i \end{pmatrix}$.

tion on IBM's 127-qubit $ibm_sherbrooke$ device demonstrates consistently high fidelity across all operational modes: non-target state preservation (93.8% \pm 0.3%), target qubit activation (94.4% \pm 0.3%), and deactivation (94.3% \pm 0.3%) [?]. This implementation eliminates SWAP requirements in linear topologies, showcasing robust performance under real-world NISQ conditions [22].

Figure 3 introduce a hardware-aware quantum circuit implementation of the Toffoli gate for linearly connected qubit architectures. The CCX gate is decomposed into a sequence of 9 CNOT gates with single-qubit rotations. Additionally, Figure 4 depicts a hardware-aware Toffoli gate implementation using ECR gates and single-qubit unitaries (U_i, W_i, V_i) , tailored for superconducting architectures with nearest-neighbor connectivity [2].

III. EXPERIMENTAL SETUP

Our experimental protocol for characterizing the Toffoli gate [24] employed a combination of benchmarking techniques (QST and QPT) with comprehensive noise analysis across IBM's superconducting quantum processors [2]. We employed both the 127-qubit $(ibm_sherbrooke)$ and $(ibm_brisbane)$ quantum architectures. Device calibration parameters, including qubit coherence times (T_1, T_2) , operating frequencies, anharmonicities, and readout fidelities, were meticulously recorded (as detailed in Section V). All hardware results were compared against idealized quantum simulations performed using IBM's $qasm_simulator$, which provided theoretical performance baselines under noiseless conditions.

A. Gate Implementation

Superconducting quantum processors operate in the NISQ era [27], where gate fidelities are fundamentally limited by decoherence processes, inter-qubit crosstalk, and calibration drift [22]. These challenges are particularly acute for the Toffoli gate [24], where the combination of multi-qubit interactions and extended gate

sequences amplifies noise susceptibility. Entangled input states such as GHZ and W states exhibit heightened vulnerability to correlated errors compared to separable states, as their non-local correlations propagate and magnify single-qubit noise channels [113].

The Toffoli gate [24] was implemented using a combination of native gate decompositions. On superconducting hardware, the gate was synthesized into echoed cross-resonance gates and single-qubit rotations, adhering to each processor's connectivity constraints. The decomposition followed the implementation shown in Figure 5.

The implementation of Toffoli gates via echoed cross-resonance protocols introduces additional calibration complexity, requiring precise tuning of microwave pulses to suppress phase errors and mitigate residual ZZ interactions [111]. This dual challenge—state-dependent noise sensitivity and exacting pulse-level calibration—underscores the delicate balance between gate functionality and fidelity in current superconducting architectures.

The unitary matrix representations for the two-qubit ECR gates are given by:

$$ECR_{q_0 \to q_1} = \begin{pmatrix} 0 & 1/\sqrt{2} & 0 & i/\sqrt{2} \\ 1/\sqrt{2} & 0 & -i/\sqrt{2} & 0 \\ 0 & i/\sqrt{2} & 0 & 1/\sqrt{2} \\ -i/\sqrt{2} & 0 & 1/\sqrt{2} & 0 \end{pmatrix}$$
(2)

$$ECR_{q_1 \to q_0} = \begin{pmatrix} 0 & 0 & 1/\sqrt{2} & i/\sqrt{2} \\ 0 & 0 & i/\sqrt{2} & 1/\sqrt{2} \\ 1/\sqrt{2} & -i/\sqrt{2} & 0 & 0 \\ -i/\sqrt{2} & 1/\sqrt{2} & 0 & 0 \end{pmatrix}$$
(3)

where $ECR_{q_i \to q_j}$ implements the echoed cross-resonance interaction with q_i acting as the control and q_j as the target. Our implementation utilizes three native single-qubit gates on the $ibm_sherbrooke$ superconducting processor (Section V): the Pauli-X gate (X) for bit-flip operations $(|0\rangle \leftrightarrow |1\rangle)$, the phase rotation gate $R_z(\varpi)$ for Z-axis rotations, and the \sqrt{X} gate for superposition generation. These gates are represented by the unitary matrices:

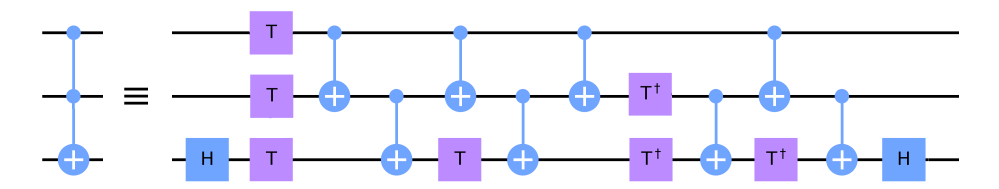


FIG. 2. A decomposition of a three-qubit CCX (Toffoli) gate requires 8 CNOT gates along with multiple single-qubit gates [25]. Optimized for quantum processors with nearest-neighbor connectivity.

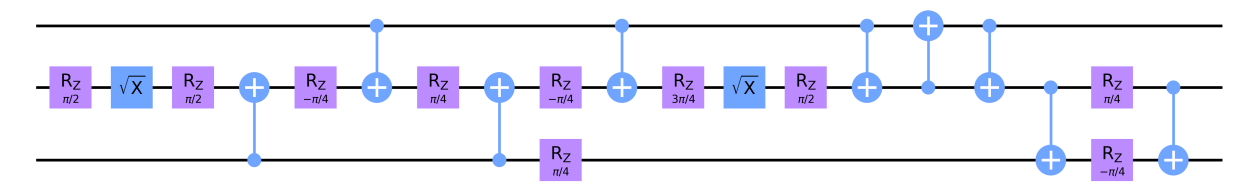


FIG. 3. Hardware-aware quantum circuit implementation of the Toffoli (CCNOT) gate for linearly connected qubit architectures. The three-qubit operation is decomposed into a sequence of 9 CNOT gates interleaved with single-qubit rotations, compiled for quantum processors with nearest-neighbor connectivity. Our implementation utilizes only the following single-qubit gates: the phase rotation gate $R_z(\varpi)$ for Z-axis rotations, and the \sqrt{X} gate for superposition generation. These gates are represented by the unitary matrices: $R_z(\varpi) = \begin{pmatrix} e^{-i\varpi/2} & 0 \\ 0 & e^{i\varpi/2} \end{pmatrix}$, $\sqrt{X} = \frac{1}{2} \begin{pmatrix} 1+i & 1-i \\ 1-i & 1+i \end{pmatrix}$.

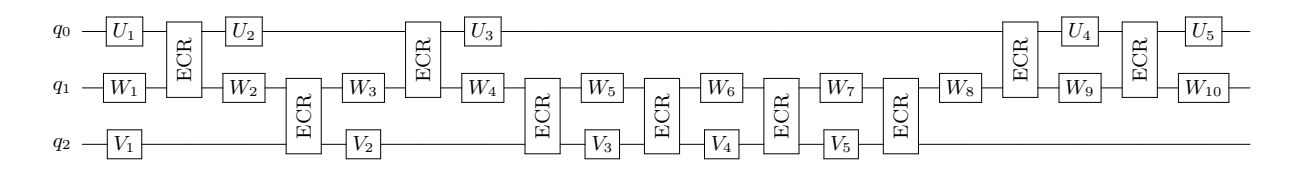


FIG. 4. Hardware-aware quantum circuit synthesis of a Toffoli gate (CCNOT) using echoed cross-resonance (ECR) gates and optimized single-qubit gates [?]. The circuit demonstrates native gate decomposition for superconducting quantum processors, with ECR operations constrained to adjacent qubits and single-qubit unitaries (U_i, W_i, V_i) compiled into IBM Quantum's native gate set.

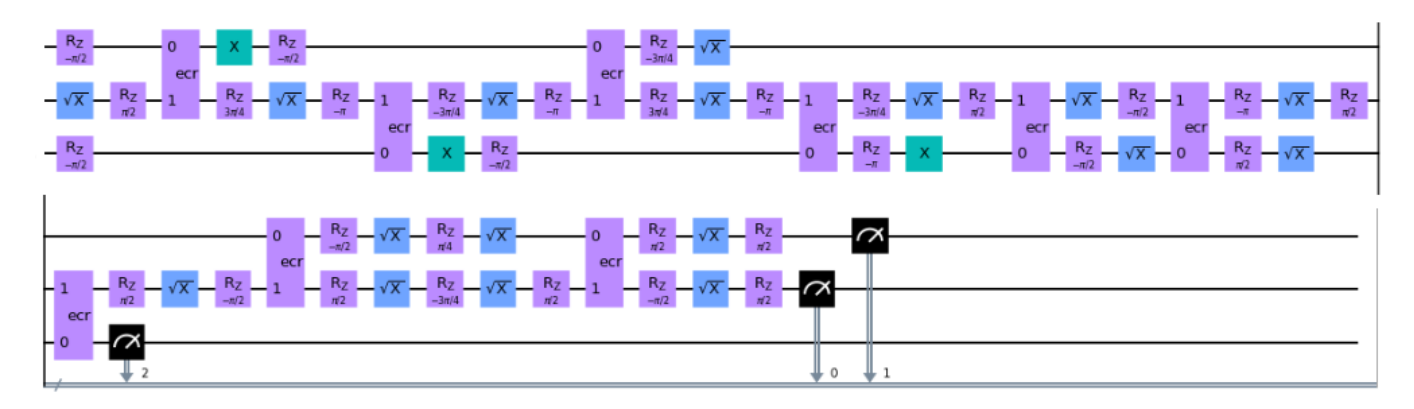


FIG. 5. Hardware-aware synthesis of a Toffoli gate using the 2-qubit ECR gates and single-qubit gates. The circuit illustrates a native gate decomposition tailored for superconducting quantum processors, compiled into IBM Quantum's native gate set, $S = \{\text{ECR, ID, R}_z(\varpi), \text{SX, X}\}$, for both the $ibm_sherbrooke$ and $ibm_brisbane$ architectures. Here, X denotes the Pauli-X gate (bit-flip, $|0\rangle \leftrightarrow |1\rangle$), $R_z(\varpi)$ represents a phase rotation around the Z-axis, and \sqrt{X} generates superpositions.

$$X = \begin{pmatrix} 0 & 1 \\ 1 & 0 \end{pmatrix}$$
 (4)
$$R_z(\varpi) = \begin{pmatrix} e^{-i\varpi/2} & 0 \\ 0 & e^{i\varpi/2} \end{pmatrix}$$
 (5)

$$\sqrt{X} = \frac{1}{2} \begin{pmatrix} 1+i & 1-i \\ 1-i & 1+i \end{pmatrix}.$$
 (6)

The $R_z(\varpi)$ gate preserves computational basis probabilities while applying phase shifts, whereas \sqrt{X} serves as the principal square root of X ($(\sqrt{X})^2 = X$), enabling coherent transitions between basis states. Together with two-qubit entangling gates, this set ($\mathcal{S}_{\mathrm{sherbrooke}} = \{ \text{ECR, ID, } R_z(\varpi), \sqrt{X}, X \}$) provides universal quantum computation capabilities on the $ibm_sherbrooke$ quantum architecture.

B. State Preparation

To evaluate the gate's performance across distinct operational regimes, we prepared three distinct classes of input states representing different entanglement configurations:

- 1. The maximally entangled GHZ state: $|\psi_{\rm GHZ}\rangle = 1/\sqrt{2}(|000\rangle + |111\rangle)$, which test coherence in maximally entangled systems.
- 2. The W state: $|\psi_{\rm W}\rangle = \frac{1}{\sqrt{3}}(|001\rangle + |010\rangle + |100\rangle)$, sensitive to asymmetric error.
- 3. A uniform superposition of all three-qubit computational basis states: $|\psi_{\text{unif}}\rangle = \frac{1}{\sqrt{8}} \sum_{i=0}^{7} |b_i\rangle$, where b_i spans $|000\rangle$ to $|111\rangle$, to assess gate performance under balanced computational basis conditions.

C. Tomography Protocol

QPT and QST are fundamental characterization techniques in quantum computing used to analyze quantum systems. QST is a procedure for reconstructing a quantum system's state from experimental measurements. The QST protocol involves: repeated measurements in different bases; state preparation before each measurement round; and computational reconstruction of the density matrix ρ from measurement statistics. The technique requires careful calibration as the number of measurements grows exponentially with system size. Various reconstruction methods have been developed, including maximum likelihood estimation and compressed sensing approaches [32, 114–119].

In our experiments, QST was employed to reconstruct the output density matrix (ρ_{out}) for each input state. Measurements were performed in the Pauli bases across all qubits, for each basis configuration, we collected 19,000 shots for $|\psi_{\text{GHZ}}\rangle$ and $|\psi_{\text{W}}\rangle$ states, and 11,000 shots for the uniform superposition $|\psi_{\text{unif}}\rangle$ to ensure statistical robustness. The state fidelity $\mathcal{F}_S(\varrho, \pounds)$ of each output state [121] was computed as shown in Equation (12) and uncertainty estimates were derived.

QPT is a key method for fully characterizing quantum operations by analyzing input-output state correlations [25, 33, 34, 126]. It reconstructs a process matrix that captures all possible quantum state transitions, enabling precise benchmarking of gate fidelities and error identification [38, 120]. Essential for validating quantum hardware and algorithms, QPT provides critical metrics for scaling reliable quantum computers [35, 36].

QPT characterizes quantum operations (gates or channels) through experimental benchmarking. Key aspects include: application to a complete set of input states; measurement of corresponding outputs; and reconstruction of the process matrix χ or Choi matrix [122]. QPT is particularly valuable for: gate validation in quantum processors [35, 36]; noise characterization in quantum circuits and calibration of experimental setups [123]. Theoretical foundations derive from the operator-sum representation [33, 124] and quantum channel theory [34, 125, 126]. Modern implementations often use the Choi-Jamiołkowski isomorphism [122, 127] for complete process characterization [38, 128].

QPT works by preparing a complete set of input states and performing measurements in various bases to reconstruct an unknown quantum process. In Qiskit's implementation [77], each qubit is initialized in one of four probe states spanning the Bloch sphere: $\{|0\rangle, |1\rangle, |\psi_{+}\rangle, |\phi_{+}\rangle\}$, corresponding to the eigenstates of the Pauli operators Z, X, and Y, respectively. Measurements are performed in each of the three Pauli bases (X, Y, and Z), using projectors defined as:

$$P_{x+} = |\psi_{+}\rangle \langle \psi_{+}|, \qquad P_{z+} = |0\rangle \langle 0|,$$

$$P_{y+} = |\phi_{+}\rangle \langle \phi_{+}|, \qquad P_{z-} = |1\rangle \langle 1|,$$
(7)

where the superposition states are given by:

$$|\psi_{\pm}\rangle = \frac{1}{\sqrt{2}}(|0\rangle \pm |1\rangle), \quad |\phi_{\pm}\rangle = \frac{1}{\sqrt{2}}(|0\rangle \pm i |1\rangle). \quad (8)$$

For a k-qubit system, quantum process tomography involves measurements in all 3^k combinations of single-qubit Pauli bases, i.e., $\{X,Y,Z\}^{\otimes k}$. To fully characterize a k-qubit quantum process, this procedure requires executing 12^k distinct quantum circuits: 4^k linearly independent input states combined with 3^k measurement settings. Each circuit must be run multiple times on actual quantum hardware to collect sufficient statistics for reliable process matrix reconstruction. This exponential scaling presents a significant resource challenge for QPT on systems with more than a few qubits, particularly on real hardware with limited shot budgets and coherence times.

The measurement results are used to construct a Choi matrix that mathematically represents the reconstructed quantum channel [122, 127]. The average gate fidelity $F_{\text{ave}}(\Im, \mathcal{W})$ is then calculated, a single number between 0 and 1, by comparing this reconstructed channel with the ideal target unitary operation [129, 130]. A fidelity

value closer to 1 indicates that the implemented quantum process more accurately matches the desired unitary operation,, with deviations from the simulator attributed to hardware-specific noise. This fidelity metric serves as a valuable tool for comparing different implementations of quantum gates [129, 130].

D. Error Analysis

The average gate fidelity $F_{\text{ave}}(\Im, \mathcal{W})$ provides a quantitative measure of how accurately a physical quantum channel \Im implements a desired unitary operation \mathcal{W} [129, 130]. This metric admits two mathematically equivalent expressions:

$$\mathcal{F}_{\text{ave}}(\Im, \mathcal{W}) = \int d\psi \, \langle \psi | \mathcal{W}^{\dagger} \Im(|\psi\rangle \langle \psi|) \mathcal{W} | \psi \rangle \qquad (9)$$

and alternatively as:

$$\mathcal{F}_{ave}(\Im, \mathcal{W}) = \frac{\Gamma \cdot \mathcal{F}_{pro}(\Im, \mathcal{W}) + 1}{\Gamma + 1}$$
 (10)

Where, $\Gamma = 2^k$ denotes the dimension of the Hilbert space for a k-qubit system, and $\mathcal{F}_{pro}(\Im, \mathcal{W})$ represents the process fidelity between the channel and target unitary.

The process fidelity $\mathcal{F}_{pro}(\Theta, \Psi)$ between arbitrary quantum channels Θ and Ψ is defined through their Choi representations:

$$\mathcal{F}_{\text{pro}}(\Theta, \Psi) = \mathcal{F}_S(\sigma_{\Theta}, \sigma_{\Psi})$$
 (11)

where: $\sigma_{\Theta} = \Xi_{\Theta}/\Gamma$ is the normalized Choi matrix of channel Θ , $\sigma_{\Psi} = \Xi_{\Psi}/\Gamma$ is the normalized Choi matrix of channel Ψ , and \mathcal{F}_{sta} denotes the standard state fidelity between density operators [121].

The underlying quantum state fidelity between density operators ϱ and \pounds is given by:

$$\mathcal{F}_S(\varrho, \pounds) = \left(\text{Tr} \sqrt{\sqrt{\varrho} \pounds \sqrt{\varrho}} \right)^2$$
 (12)

Thus, $\mathcal{F}_{\text{pro}}(\Theta, \Psi)$ can be written as:

$$\mathcal{F}_{\text{pro}}(\Theta, \Psi) = \left(\text{Tr} \sqrt{\sqrt{\sigma_{\Theta}} \, \sigma_{\Psi} \sqrt{\sigma_{\Theta}}} \right)^2 \tag{13}$$

When comparing a channel to a unitary operation \mathcal{W} , this reduces to:

$$\mathcal{F}_{\text{pro}}(\Im, \mathcal{W}) = \frac{\text{Tr}(S_{\mathcal{W}}^{\dagger} S_{\Im})}{\Gamma^2}$$
 (14)

where S_{\Im} and $S_{\mathcal{W}}$ denote the superoperator representations in the Pauli basis. If the target channel Ψ has a pure state $\sigma_{\Psi} = |\psi_{\Psi}\rangle\langle\psi_{\Psi}|$, the fidelity simplifies to:

$$\mathcal{F}_{\text{pro}}(\Theta, \Psi) = \langle \psi_{\Psi} | \sigma_{\Theta} | \psi_{\Psi} \rangle \tag{15}$$

IV. RESULTS AND DISCUSSION

The fidelities from QST experiments represent how closely the actual output state of our Toffoli gate matches the ideal expected state for specific input classes (GHZ, W, uniform superposition). Our QST experiments reveal critical insights into the performance of the Toffoli gate [24] across different input states and hardware platforms. The GHZ state—a critical benchmark for multi-qubit entanglement—showed perfect behavior in noise-free quantum simulation (98.4% state fidelity), with slight degradation in noisy quantum emulation (81.470% state fidelity), but suffered dramatic degradation on hardware. When executed on *ibm_sherbrooke*, the same gate operation yielded just 56.4% state fidelity (Figure 6).

The W state followed a similar pattern, maintaining 98.7% state fidelity in noise-free quantum simulation, 79.900% state fidelity in noisy environment, and dropping to 63.7% on quantum hardware (Figure 7), with its complex superposition particularly vulnerable to asymmetric noise. Interestingly, the uniform superposition state demonstrated the highest noise-free quantum simulation state fidelity (99.5%) and 85.469% state fidelity in noisy settings, but still faced substantial challenges on $ibm_brisbane$, achieving only 61.2% state fidelity (Figure 8). This universal performance drop across all test states highlights fundamental limitations in current NISQ-era hardware.

QPT quantified the gate's operational limitations with even starker results. While the $qasm_simulator$ showed near-ideal process fidelity (99.0%), noisy emulation revealed how quickly performance degrades (80.2% process fidelity). The missing hardware process fidelity measurements would likely show even more severe degradation, consistent with our state tomography results. Figure 9 presents results from our QPT characterization of the Toffoli gate, including the reconstructed quantum process matrices along with their corresponding process fidelities. The protocol requires 12^k distinct circuit configurations for a k-qubit operation. For the Toffoli gate (k = 3), we executed each of the 12^3 circuits with 11,000 measurement shots, resulting in a total of 1.9008×10^7 individual measurements to ensure statistically reliable results.

The complete QPT of the 3-qubit Toffoli gate [24]—requiring 1,728 quantum circuits and 19,008,000 individual measurements—was conducted using both the noise-free qasm_simulator and a noisy quantum emulator, as real hardware execution was infeasible due to experimental constraints. The noisy emulator replicates real quantum hardware by integrating experimentally measured noise profiles, including gate errors, readout errors, and decoherence times. This approach provides a realistic approximation of how QPT behaves on actual IBM quantum processors under realistic noise conditions. By leveraging this emulation framework, we obtain rigorous yet experimentally tractable insights into gate fidelity while avoiding the prohibitive resource overhead of performing full QPT on

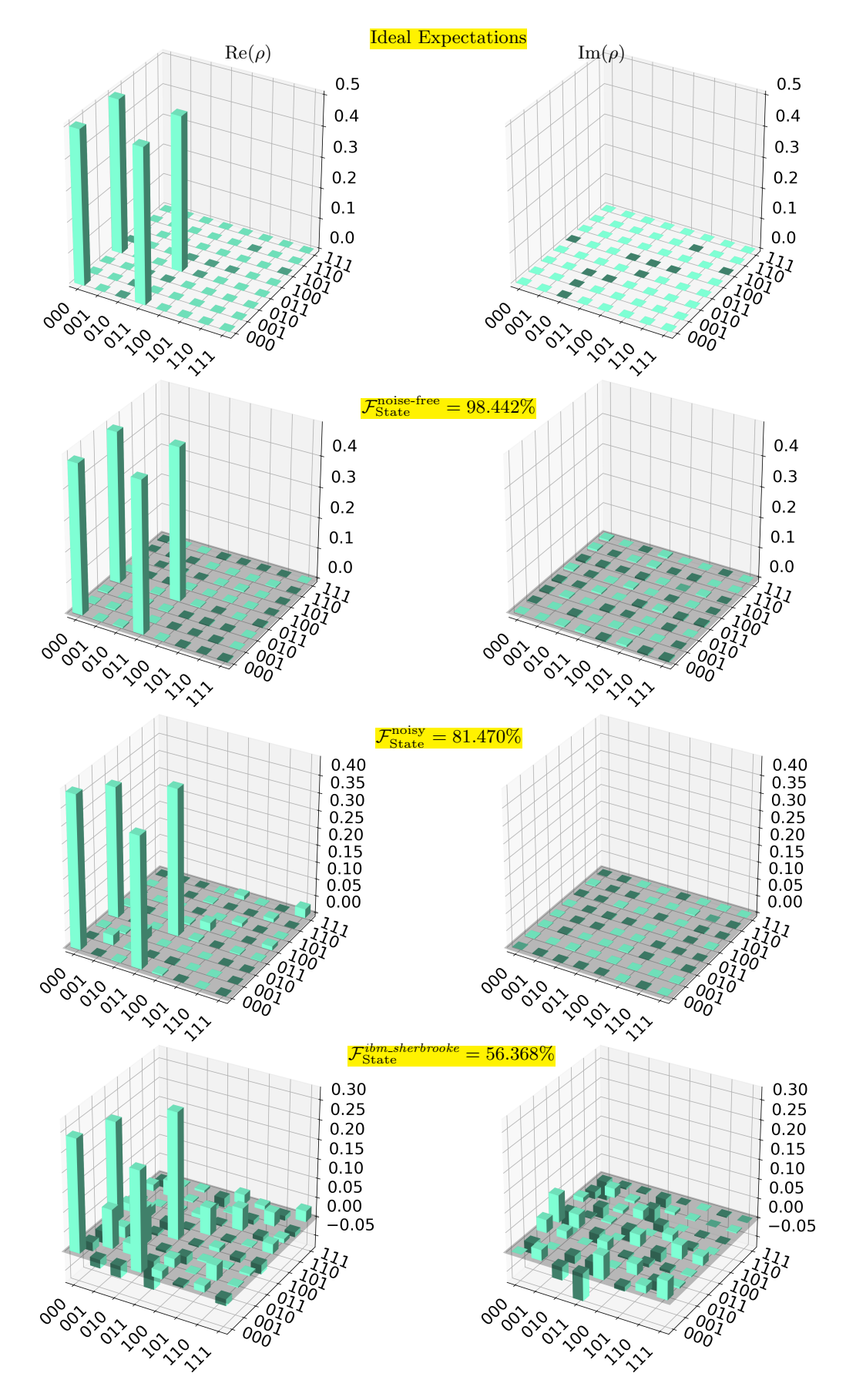


FIG. 6. QST of the Toffoli gate with input state prepared as the maximally entangled GHZ state $(\frac{1}{\sqrt{2}}(|000\rangle + |111\rangle))$. The QST measurements were conducted with 19,000 shots in each different operational environment. The results demonstrate substantial variations in gate fidelity across different operational environments, achieving fidelities of 98.442% (noise-free), 81.470% (noisy emulation), and 56.368% (real hardware, $ibm_sherbrooke$) with hardware implementations exhibiting particular sensitivity to initial state preparation conditions.

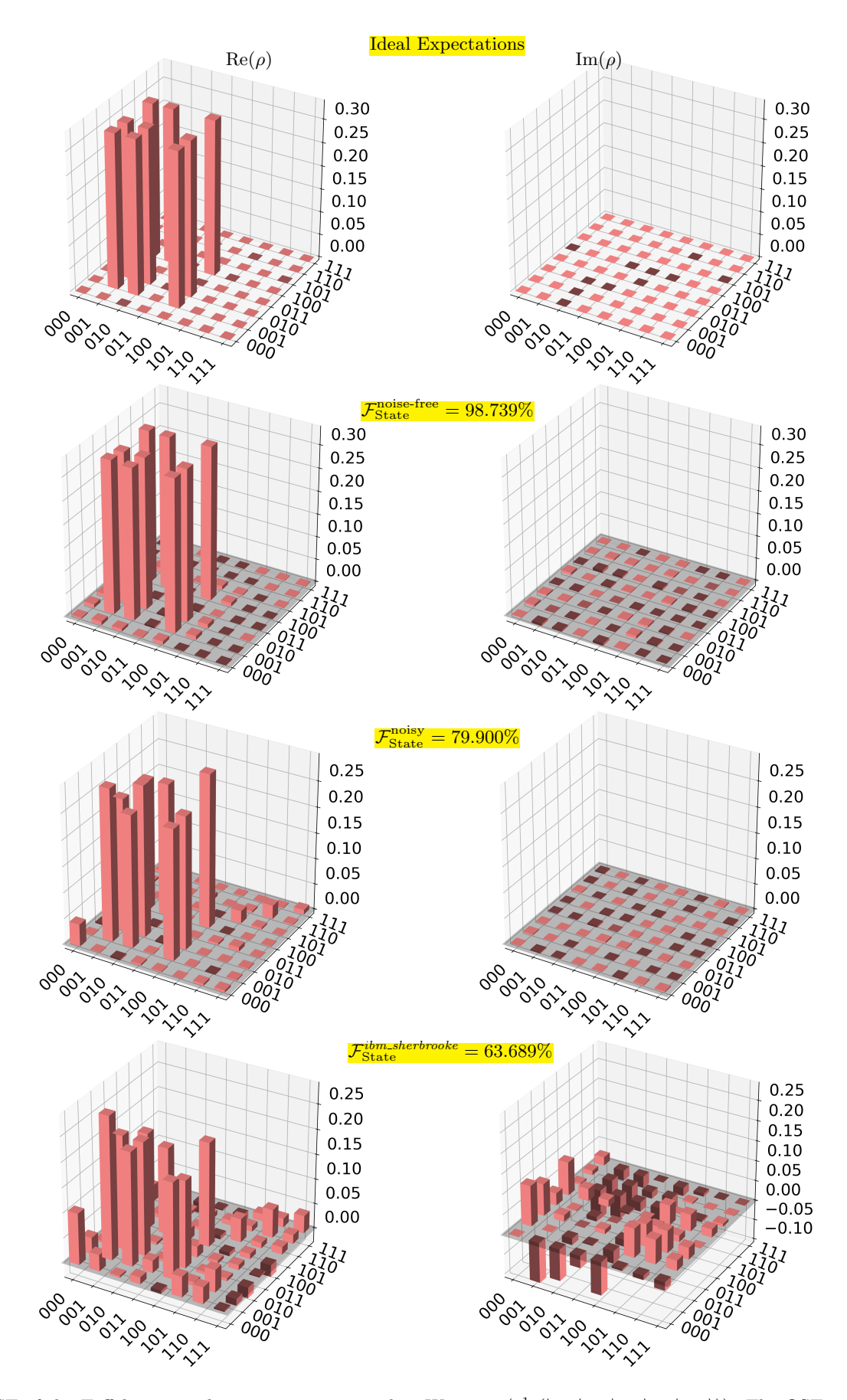


FIG. 7. QST of the Toffoli gate with input state prepared as W states $(\frac{1}{\sqrt{3}}(|001\rangle + |010\rangle + |100\rangle))$. The QST measurements were conducted with 19,000 shots in each different operational environment. The results demonstrate substantial variations in gate fidelity across different operational environments, achieving fidelities of 98.739% (noise-free), 79.900% (noisy emulation), and 63.689% (real hardware, $ibm_sherbrooke$) with hardware implementations exhibiting particular sensitivity to initial state preparation conditions.

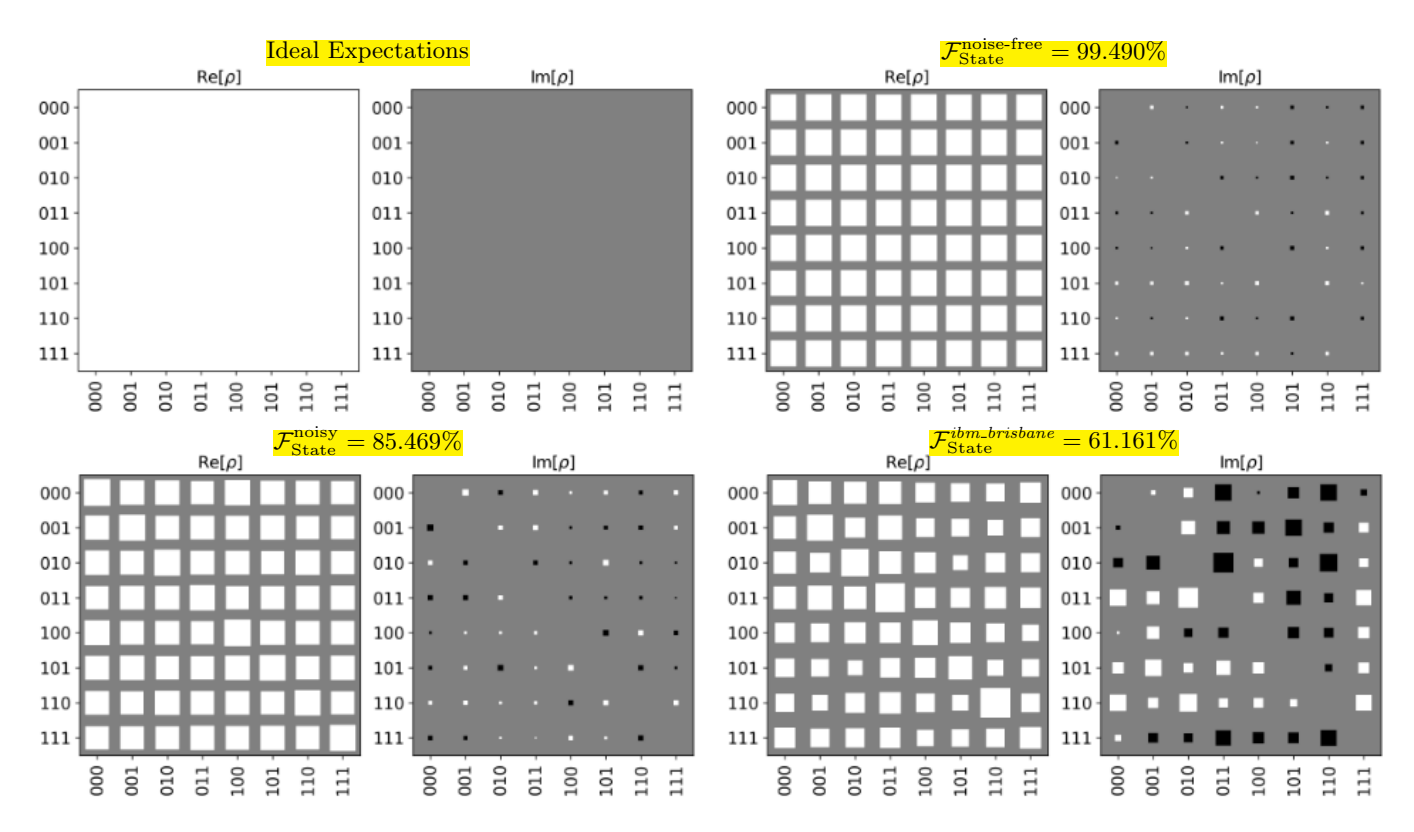


FIG. 8. QST of the Toffoli gate with input state prepared as a uniform superposition of all three-qubit computational basis states $(\frac{1}{\sqrt{8}}\sum_{i=0}^{7}|b_i\rangle)$, where b_i spans $|000\rangle$ to $|111\rangle)$. The QST measurements were conducted with 11,000 shots in each different operational environment. The results demonstrate substantial variations in gate fidelity across different operational environments, achieving fidelities of 99.490% (noise-free), 85.469% (noisy emulation), and 61.161% (real hardware, $ibm_brisbane$) with hardware implementations exhibiting particular sensitivity to initial state preparation conditions.

physical quantum devices.

Table I presents an analysis of Toffoli gate statedependent fidelity metrics across different operational environments on IBM's 127-qubit ibm_sherbrooke and *ibm_brisbane* quantum processors. Through rigorous QST and QPT protocols, we evaluated gate performance for three distinct input state classes: GHZ states, W states, and uniform superpositions. The QST measurements were conducted with 19,000 shots for GHZ and W state analyses, while the uniform superposition characterization employed 11,000 shots to ensure statistically robust results. Corresponding QPT investigations were conducted with 11,000 shots for reliable process fidelity estimation. The results demonstrate substantial variations in gate fidelity across different input states and operational environments, with hardware implementations exhibiting particular sensitivity to initial state preparation conditions, highlighting the considerable implementation challenges in current NISQ processors.

V. QUANTUM HARDWARE PERFORMANCE

Our experiments were conducted on two IBM's Eagle r3 superconducting quantum processors: *ibm_sherbrooke*,

 $ibm_brisbane.$ Both state-of-the-art 127-qubit quantum processors implement the ECR gates as their native entangling operations, with median error rates of 7.56×10^{-3} (ibm_sherbrooke) and 8.32×10^{-3} (ibm_brisbane) respectively. Isolated two-qubit gate fidelities reached 2.92×10^{-3} (ibm_sherbrooke) and $3.16 \times$ 10^{-3} (*ibm_brisbane*) as measured by randomized benchmarking, while layered error per logical gate (EPLG) for 100-qubit chains was 1.35×10^{-2} and 1.65×10^{-2} respectively. The systems demonstrated distinct performance characteristics: ibm_sherbrooke exhibited median coherence times $(T_1 = 272.21 \ \mu s, T_2 = 188.10 \ \mu s)$ and lower gate errors, making it preferable for deep circuits, whereas ibm_brisbane achieved higher computational throughput (180K vs 150K CLOPS), benefiting real-time applications. Both systems shared identical basis gate sets ($S = \{ECR, ID, R_z(\varpi), \sqrt{X}, X\}$) and support pulse-level control capabilities, with median single-qubit (\sqrt{X}) and readout errors below 2.36×10^{-4} and 1.71×10^{-2} respectively. This measured performance characteristics (as of 14 April 2025) represents the state-of-the-art performance for NISQ-era superconducting quantum processors.

The Toffoli gate [24] implementations were characterized across three distinct experimental configurations,

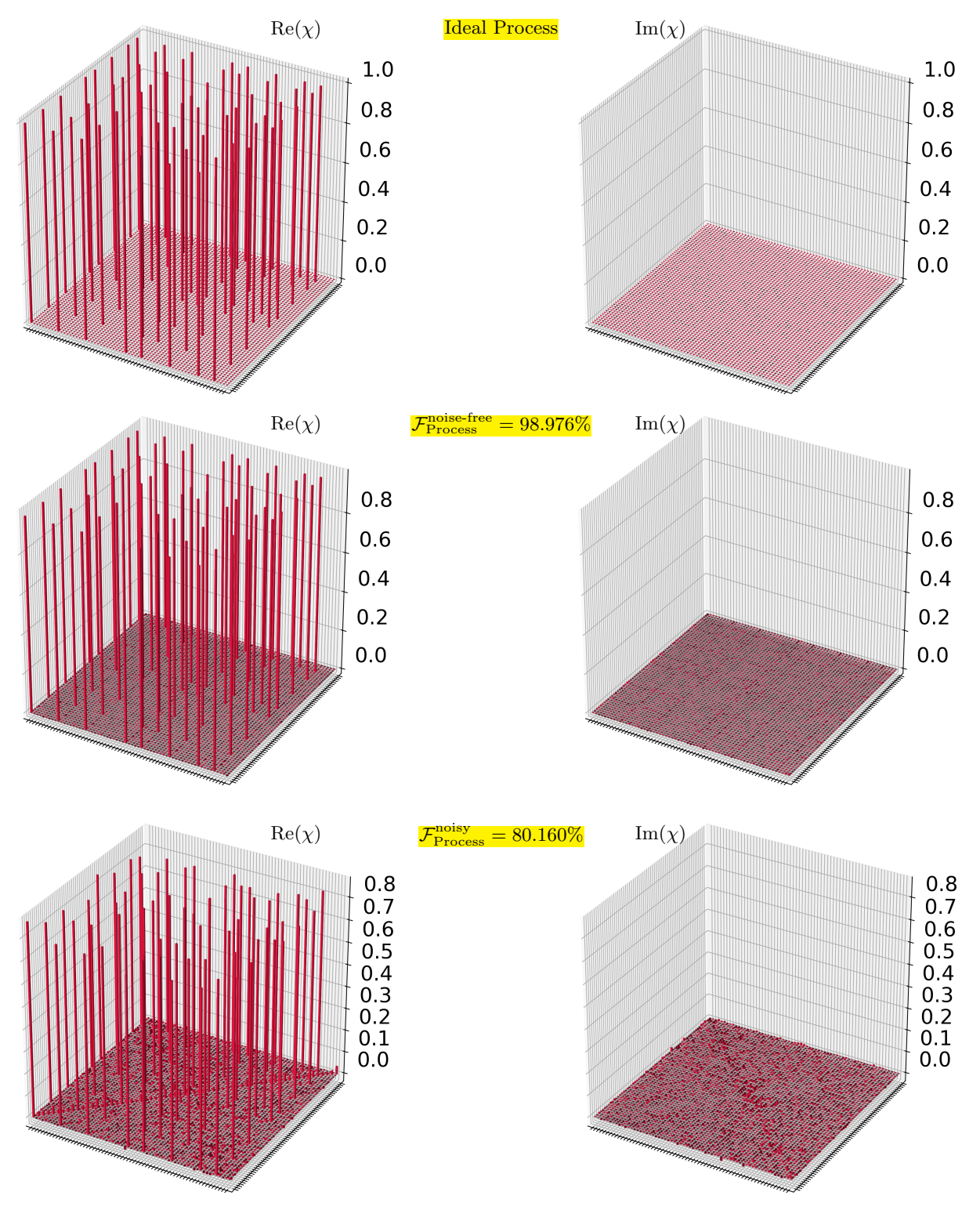


FIG. 9. QPT experiments of the Toffoli gate. While the *qasm_simulator* showed near-ideal process fidelity (99.0%), noise-aware quantum emulation revealed how quickly performance degrades (80.2% process fidelity).

with comprehensive qubit metrics documented in Tables s II–IV. Tables II and III detail $ibm_sherbrooke$'s behavior for entangled input states, with Table II quantifying GHZ-state operations ($|\psi_{\text{GHZ}}\rangle$), and Table III

capturing W-state dynamics $(|\psi_{\rm W}\rangle)$. Table IV presents $ibm_brisbane$'s performance during uniform superposition tests $(|\psi_{\rm unif}\rangle)$, revealing median coherence times under balanced state preparation of $T_1=242.989~\mu{\rm s}$ and

TABLE I. Fidelity metrics obtained form a systematic characterization of the Toffoli gate on IBM's 127-qubit *ibm_sherbrooke* and *ibm_brisbane* processors using quantum state tomography (QST) and quantum process tomography (QPT). We measure the gate's fidelity for three input state classes (GHZ, W, and uniform superpositions). All QST measurements used 19,000 shots except uniform superposition (11,000 shots). QPT experiments employed 11,000 shots. Our results demonstrate significant fidelity variations across different input states and environments, with hardware implementations showing particular sensitivity to state preparation. The process fidelity maintains 0.990 in simulation but drops to 0.802 under noisy conditions, revealing substantial implementation challenges for three-qubit gates on current superconducting quantum processors.

Input State	QST experiments				
input state	Noise-free settings ^a	Noise-aware quantum emulation	Real quantum hardware		
$GHZ \left(\frac{1}{\sqrt{2}} (000\rangle + 111\rangle) \right)$	98.442%	81.470%	56.368% (ibm_sherbrooke)		
$W(\frac{1}{\sqrt{3}}(001\rangle + 010\rangle + 100\rangle))$	98.739%	79.900%	$ 63.689\% (ibm_sherbrooke) $		
Uniform superpositions $(\frac{1}{\sqrt{8}}\sum_{x\in\{0,1\}^3} x\rangle)$	99.490%	85.469%	$61.161\% (ibm_brisbane)$		
QPT (Process Fidelity)	99.0 %	80.2%	_b		

^a "Noise-free" refers to an idealized quantum circuit simulated with finite-shot sampling, hence the fidelity < 100% is due to statistical (sampling) error, not physical noise.

b Full QPT of the Toffoli gate—requiring 1,728 circuits—was executed using both noise-free simulation and noise-aware emulation, as real hardware execution was constrained by runtime and coherence limitations.

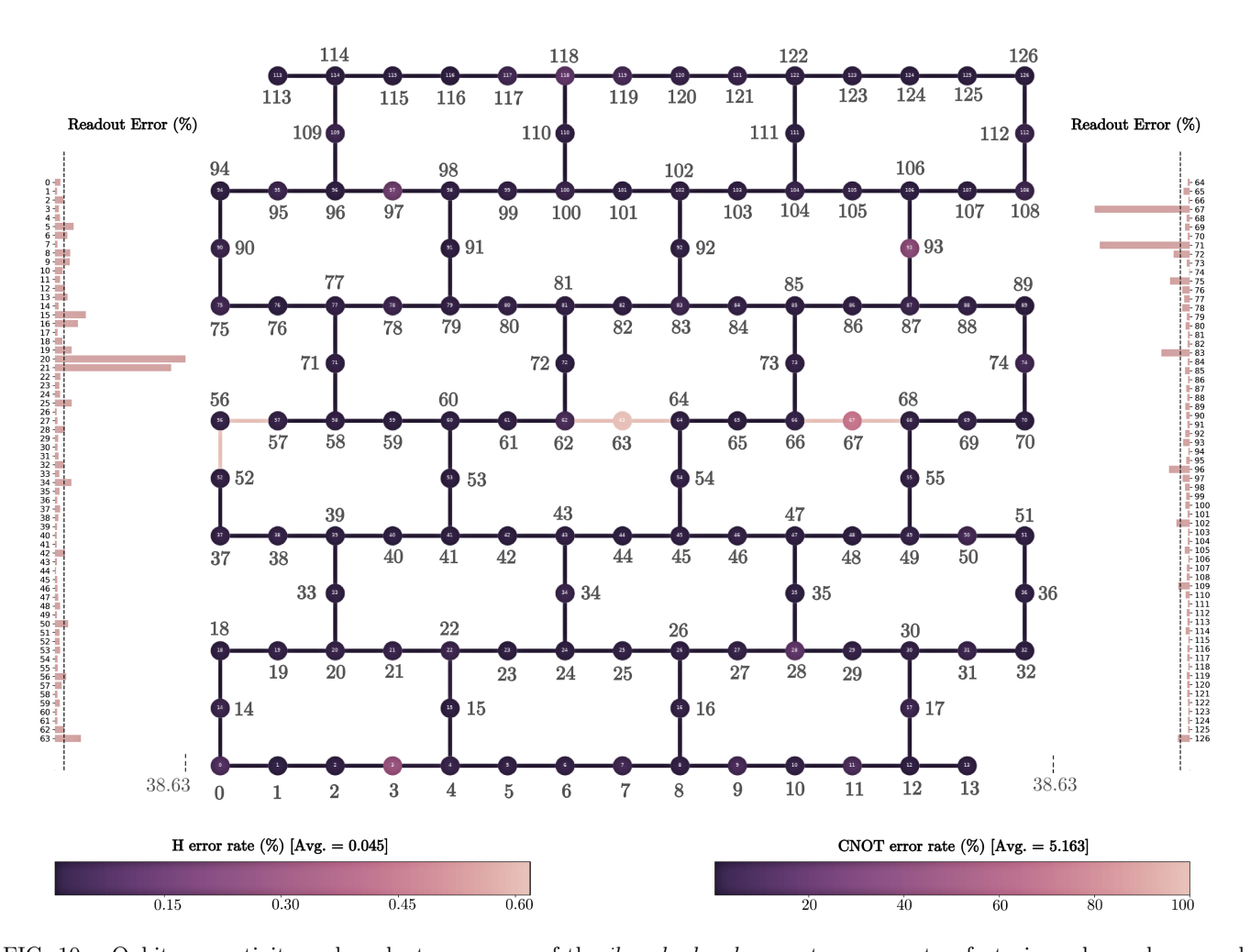


FIG. 10. Qubit connectivity and readout error map of the *ibm_sherbrooke* quantum computer, featuring a heavy-hexagonal architecture where each qubit (circles) connects to 2-3 neighbors. With qubit-specific readout error rates, demonstrating performance variations across the device. The layout reflects the architecture of IBM's *Eagle* r3 processor, identical layout implemented in the *ibm_brisbane* quantum system. This visualization was regenerated from [90] under a Creative Commons Attribution 4.0 International License (https://creativecommons.org/licenses/by/4.0/).

TABLE II. Statistical summary of qubit performance metrics for $ibm_sherbrooke$ during Toffoli gate characterization using GHZ states. Data obtained through QST with input state $|\psi_{\rm GHZ}\rangle = \frac{1}{\sqrt{2}}(|000\rangle + |111\rangle)$. Metrics were recorded during QST execution to ensure operational relevance. Measured parameters, including coherence times (T_1, T_2) , qubit frequencies $(\omega/2\pi)$, anharmonicities $(\alpha/2\pi)$, probability of misclassifying $|1\rangle$ as $|0\rangle$ $(P(|0\rangle | |1\rangle)$), probability of misclassifying $|0\rangle$ as $|1\rangle$ $(P(|1\rangle | |0\rangle)$), readout errors (ϵ_r) , and readout length (τ_r) . Metrics were recorded during QST execution to ensure operational relevance. The table presents the mean, standard deviation (std), minimum (min), quartiles (25%, 50%, 75%), and maximum (max) values for each measured parameter across the qubit ensemble. All values are reported with their original units and precision.

Metric	Mean	\mathbf{StdDev}	Min	25 %	Median	75 %	Max
$T_1 \; (\mu \mathrm{s})$	268.794016	92.019836	26.800000	207.245000	280.110000	332.410000	493.220000
$T_2 (\mu s)$	188.904803	105.945732	16.930000	89.940000	185.350000	268.510000	437.850000
$\omega/2\pi$ (GHz)	4.787043	0.107821	4.455300	4.726350	4.792700	4.854450	5.057500
$\alpha/2\pi$ (GHz)	-0.310447	0.005477	-0.324300	-0.312300	-0.310900	-0.309700	-0.271900
ϵ_r	0.027813	0.059267	0.002400	0.007250	0.011100	0.022500	0.446800
$P(0\rangle 1\rangle)$	0.030585	0.065054	0.002600	0.007900	0.012400	0.023800	0.457000
$P(1\rangle 0\rangle)$	0.025009	0.056593	0.001400	0.004900	0.008400	0.020300	0.436600
$\tau_r \; (\mathrm{ns})$	1.24444×10^3	0.000000	1.24444×10^3				

TABLE III. Statistical summary of qubit performance metrics for *ibm_sherbrooke* during Toffoli gate characterization using W states. Data obtained through QST with input state $|\psi_{\rm W}\rangle = \frac{1}{\sqrt{3}}(|001\rangle + |010\rangle + |100\rangle)$.

Metric	Mean	StdDev	Min	25 %	Median	75 %	Max
$T_1 \; (\mu \mathrm{s})$	266.228189	82.446799	26.800000	218.245000	268.070000	315.960000	493.220000
$T_2 \; (\mu \mathrm{s})$	189.185197	108.075822	1.800000	94.105000	189.180000	273.685000	437.850000
$\omega/2\pi$ (GHz)	4.790008	0.109124	4.455000	4.732000	4.794000	4.859500	5.058000
$\alpha/2\pi$ (GHz)	-0.311047	0.009131	-0.393000	-0.312000	-0.311000	-0.310000	-0.272000
ϵ_r	0.029228	0.059433	0.002000	0.007500	0.012000	0.024500	0.453000
$P(0\rangle 1\rangle)$	0.032457	0.065516	0.003000	0.008000	0.013000	0.023500	0.456000
$P(1\rangle 0\rangle)$	0.025504	0.055825	0.001000	0.005000	0.010000	0.020500	0.451000
τ_r (ns)	1.24444×10^3	0.000000	1.24444×10^3				

TABLE IV. Statistical summary of performance metrics for $ibm_brisbane$ recorded during QST execution to ensure operational relevance. Data obtained through QST for Toffoli gate with uniform superpositions: with input state $|\psi_{\rm unif}\rangle = \frac{1}{\sqrt{8}} \sum_{x=0}^{7} |x\rangle$, where $|x\rangle$ represents 3-bit computational basis states.

Metric	Mean	StdDev	Min	25 %	Median	75 %	Max
$T_1 (\mu s)$	232.758268	85.470333	11.416000	171.976500	242.989000	292.665500	443.132000
$T_2 (\mu s)$	157.844110	92.724177	16.724000	80.348500	151.424000	223.955500	395.372000
$\omega/2\pi$ (GHz)	4.896178	0.109273	4.609670	4.821195	4.905600	4.971760	5.117740
$\alpha/2\pi$ (GHz)	-0.308664	0.005384	-0.359050	-0.309740	-0.308420	-0.307400	-0.289810
ϵ_r	0.024203	0.036601	0.005200	0.009150	0.012500	0.020400	0.253900
$P(0\rangle 1\rangle)$	0.023783	0.034836	0.005400	0.009700	0.014000	0.021100	0.253400
$P(1\rangle 0\rangle)$	0.024624	0.043895	0.003000	0.007600	0.011600	0.020000	0.345200
$\tau_r \; (\mathrm{ns})$	4.000×10^3	0.000000	4.000×10^{3}	4.000×10^3	4.000×10^3	4.000×10^3	4.000×10^3

 $T_2=151.424~\mu s$, with isolated ECR gate errors reaching 3.16×10^{-3} . This dataset enables comparative analysis of error propagation across different entanglement regimes while maintaining consistent operational conditions.

Figure 10 shows the qubit connectivity and readout errors of IBM's 127-qubit $ibm_sherbrooke$ processor (Eagle r3 architecture), which shares the same layout as $ibm_brisbane$. Figure 11 presents a comparison of qubit performance metrics across three quantum processor configurations, measured during Toffoli gate characterization. Data were collected under three distinct input states: GHZ states ($|\psi_{\rm GHZ}\rangle$) and W states ($|\psi_{\rm W}\rangle$) on $ibm_sherbrooke$, and uniform superpositions ($|\psi_{\rm unif}\rangle$) on $ibm_brisbane$. Whiskers indicate the 5th–95th percentile ranges across all 127 qubits, demonstrating state-dependent performance characteristics in superconducting quantum hardware.

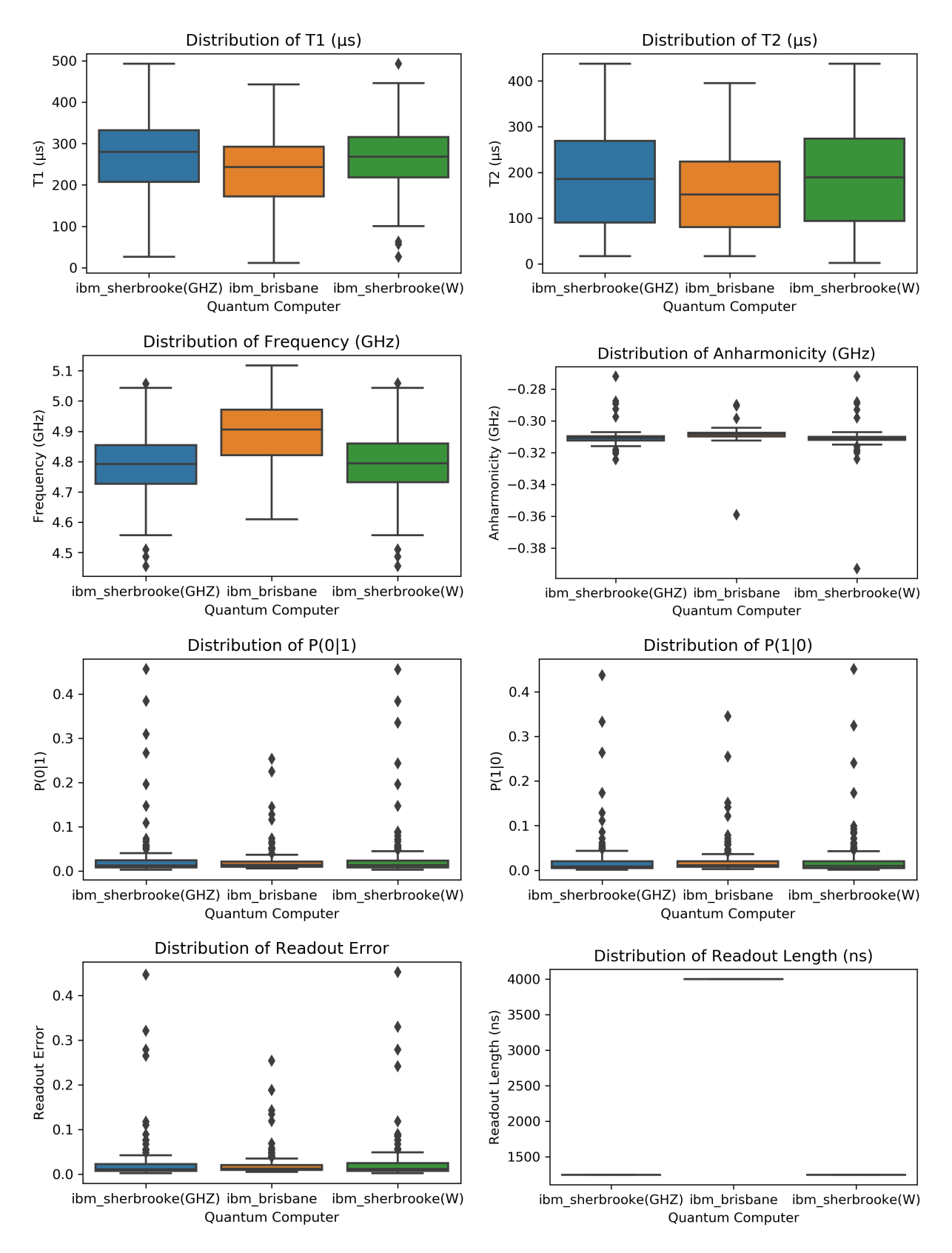


FIG. 11. Comparative distributions of qubit performance metrics across the quantum processors. Boxplots show measured values (rows from upper left to lower right) of: coherence times $(T_1, T_2 \text{ in } \mu \text{s})$, transition frequencies (f_{01}) and anharmonicities $(\alpha, \text{both in GHz})$, readout error probabilities (P(0|1), P(1|0)), and readout errors and pulse lengths (ns). Data were collected during Toffoli gate characterization using three distinct input states: GHZ states $(|\psi_{\text{GHZ}}\rangle = \frac{1}{\sqrt{2}}(|000\rangle + |111\rangle))$ on $ibm_sherbrooke$, W states $(|\psi_{\text{W}}\rangle = \frac{1}{\sqrt{3}}(|001\rangle + |010\rangle + |100\rangle))$ on $ibm_sherbrooke$, and uniform superpositions $(|\psi_{\text{unif}}\rangle = \frac{1}{\sqrt{8}}\sum_{x=0}^{7}|x\rangle)$ on $ibm_brisbane$. Whiskers indicate 5th-95th percentiles of the distributions across all 127 qubits.

VI. CONCLUSION

This study presents a rigorous experimental characterization of the Toffoli gate's performance on state-ofthe-art superconducting quantum processors, combining QST and QPT to uncover the intricate relationship between input states, gate fidelity, and hardware-specific noise, revealing fundamental insights into the challenges of executing three-qubit operations in the NISQ era. We evaluate the gate performance across entangled and separable input states using QST and QPT. We evaluate the gate's fidelity for three classes of input states: Greenberger-Horne-Zeilinger states ($|\psi_{\text{GHZ}}\rangle$), achieving fidelities of 98.442% (noise-free quantum simulation), 81.470% (noise-aware quantum emulation), and 56.368% (real quantum hardware); W states ($|\psi_{\rm W}\rangle$), yielding state fidelities of 98.739%, 79.900%, and 63.689% under the same conditions, while a uniform superposition of all three-qubit computational basis states ($|\psi_{\text{unif}}\rangle$), reaching 99.490%, 85.469%, and 61.161%, respectively.

The state-dependent fidelity patterns we observed are particularly revealing. Our quantum tomography-based approach demonstrates that while noise-free quantum simulations predict near-perfect operation (98.4 – 99.5% state fidelity), and noise-aware quantum emulation predict 79.90-85.469% state fidelity; actual hardware performance remains severely limited, achieving 56-64% state fidelity across different input state classes. Additionally, QPT experiments reveal a process fidelity of 98.976% and 80.160% in noise-free and noise-aware quantum emulation, respectively. This precipitous decline underscores the substantial challenges facing NISQ-era quantum computing.

The observed performance variations across different input states—particularly the pronounced state fidelity degradation in entangled states compared to simpler superpositions—highlight the complex interplay between quantum state preparation and gate implementation. The demonstrated state-dependent performance characteristics suggest that algorithm designers have to carefully consider input state selection and may need to develop specialized error mitigation strategies for operations involving three-qubit gates.

These findings provide valuable insights into the operational limitations of complex quantum gates on near-term quantum hardware. As quantum processors scale, the insights gained here will inform the development of robust, application-specific gate implementations—bridging the gap between theoretical potential and practical execution in the NISQ era and beyond.

ACKNOWLEDGMENTS

"We acknowledge the use of IBM Quantum's computers for this research. However, the views and conclusions expressed by the author are their own and do not necessarily reflect IBM Quantum's official policy or position."

DECLARATIONS

Ethical approval and consent to participate

Not applicable.

Consent for publication

The author have approved the publication. This research did not involve any human, animal or other participants.

Availability of supporting data

The datasets generated during and/or analyzed during the current study are included within this article.

Competing interests

The author declares no competing interests.

Funding

This article is published open access under the agreement between Springer Nature and the Science, Technology & Innovation Funding Authority (STDF), in cooperation with the Egyptian Knowledge Bank (EKB). The author declares that no funding, grants, or other forms of financial support were received at any stage of this research.

Authors' contributions

"M. AbuGhanem: conceptualization, methodology, resources, quantum programming, experimental implementations on IBM Quantum's quantum computers, data curation, formal analysis, statistical analysis, visualization, investigation, validation, writing, reviewing and editing. The author has approved the final manuscript."

T. D. Ladd, F. Jelezko, R. Laflamme, Y. Nakamura, C. Monroe , J. L. O'Brien, Quantum computers. *Nature* 464, 45–53 (2010).

^[2] M. AbuGhanem, IBM quantum computers: evolution, performance, and future directions. J Supercomput 81, 687 (2025).

- [3] P. Dirac, The principles of quantum mechanics. Clarendon Press, Oxford (1930).
- [4] M. AbuGhanem, "Properties of some quantum computing models," Master's Thesis, Fac. Sci., Ain Shams Univ. (2019).
- [5] Frank Arute, Kunal Arya, Ryan Babbush, Dave Bacon, Joseph C. Bardin, Rami Barends, Rupak Biswas, Sergio Boixo, Fernando G. S. L. Brandao, David A. Buell, Brian Burkett, Yu Chen, Zijun Chen, Ben Chiaro, Roberto Collins, William Courtney, Andrew Dunsworth, Edward Farhi, Brooks Foxen, Austin Fowler, Craig Gidney, Marissa Giustina, Rob Graff, Keith Guerin, Steve Habegger, Matthew P. Harrigan, Michael J. Hartmann, Alan Ho, Markus Hoffmann, Trent Huang, Travis S. Humble, Sergei V. Isakov, Evan Jeffrey, Zhang Jiang, Dvir Kafri, Kostyantyn Kechedzhi, Julian Kelly, Paul V. Klimov, Sergey Knysh, Alexander Korotkov, Fedor Kostritsa, David Landhuis, Mike Lindmark, Erik Lucero, Dmitry Lyakh, Salvatore Mandrà, Jarrod R. McClean, Matthew McEwen, Anthony Megrant, Xiao Mi, Kristel Michielsen, Masoud Mohseni, Josh Mutus, Ofer Naaman, Matthew Neeley, Charles Neill, Murphy Yuezhen Niu, Eric Ostby, Andre Petukhov, John C. Platt, Chris Quintana, Eleanor G. Rieffel, Pedram Roushan, Nicholas C. Rubin, Daniel Sank, Kevin J. Satzinger, Vadim Smelyanskiy, Kevin J. Sung, Matthew D. Trevithick, Amit Vainsencher, Benjamin Villalonga, Theodore White, Z. Jamie Yao, Ping Yeh, Adam Zalcman, Hartmut Neven and John M. Martinis, Quantum supremacy using a programmable superconducting processor, *Nature* **574**, 505–510, (2019).
- [6] Yulin Wu, Wan-Su Bao, Sirui Cao, Fusheng Chen, Ming-Cheng Chen, Xiawei Chen, Tung-Hsun Chung, Hui Deng, Yajie Du, Daojin Fan, Ming Gong, Cheng Guo, Chu Guo, Shaojun Guo, Lianchen Han, Linvin Hong, He-Liang Huang, Yong-Heng Huo, Liping Li, Na Li, Shaowei Li, Yuan Li, Futian Liang, Chun Lin, Jin Lin, Haoran Qian, Dan Qiao, Hao Rong, Hong Su, Lihua Sun, Liangyuan Wang, Shiyu Wang, Dachao Wu, Yu Xu, Kai Yan, Weifeng Yang, Yang Yang, Yangsen Ye, Jianghan Yin, Chong Ying, Jiale Yu, Chen Zha, Cha Zhang, Haibin Zhang, Kaili Zhang, Yiming Zhang, Han Zhao, Youwei Zhao, Liang Zhou, Qingling Zhu, Chao-Yang Lu, Cheng-Zhi Peng, Xiaobo Zhu, Jian-Wei Pan, Strong quantum computational advantage using a superconducting quantum processor, Phys. Rev. Lett. **127**, 180501 (2021).
- [7] M. AbuGhanem, "Information processing at the speed of light." Front. Optoelectron. 17, 33 (2024).
- [8] Qingling Zhu, Sirui Cao, Fusheng Chen, Ming-Cheng Chen, Xiawei Chen, Tung-Hsun Chung, Hui Deng, Yajie Du, Daojin Fan, Ming Gong, Cheng Guo, Chu Guo, Shaojun Guo, Lianchen Han, Linyin Hong, He-Liang Huang, Yong-Heng Huo, Liping Li, Na Li, Shaowei Li, Yuan Li, Futian Liang, Chun Lin, Jin Lin, Haoran Qian, Dan Qiao, Hao Rong, Hong Su, Lihua Sun, Liangyuan Wang, Shiyu Wang, Dachao Wu, Yulin Wu, Yu Xu, Kai Yan, Weifeng Yang, Yang Yang, Yangsen Ye, Jianghan Yin, Chong Ying, Jiale Yu, Chen Zha, Cha Zhang, Haibin Zhang, Kaili Zhang, Yiming Zhang, Han Zhao, Youwei Zhao, Liang Zhou, Chao-Yang Lu, Cheng-Zhi Peng, Xiaobo Zhu, Jian-Wei Pan, Quantum computational advantage via 60-qubit 24-cycle random circuit sampling, Science Bulletin 67,3, (2022).

- [9] Youngseok Kim, Andrew Eddins, Sajant Anand, Ken Xuan Wei, Ewout van den Berg, Sami Rosenblatt, Hasan Nayfeh, Yantao Wu, Michael Zaletel, Kristan Temme and Abhinav Kandala, Evidence for the utility of quantum computing before fault tolerance. *Nature* 618:500–505 (2023).
- [10] M. AbuGhanem and H. Eleuch, "NISQ computers: a path to quantum supremacy," *IEEE Access*, 12, 102941-102961 (2024).
- [11] Rajeev Acharya, Dmitry A. Abanin, Laleh Aghababaie-Beni, Igor Aleiner, Trond I. Andersen, Markus Ansmann, Frank Arute, Kunal Arya, Abraham Asfaw, Nikita Astrakhantsev, Juan Atalaya, Ryan Babbush, Dave Bacon, Brian Ballard, Joseph C. Bardin, Johannes Bausch, Andreas Bengtsson, Alexander Bilmes, Sam Blackwell, Sergio Boixo, Gina Bortoli, Alexandre Bourassa, Jenna Bovaird, Leon Brill, Michael Broughton, David A. Browne, Brett Buchea, Bob B. Buckley, David A. Buell, Tim Burger, Brian Burkett, Nicholas Bushnell, Anthony Cabrera, Juan Campero, Hung-Shen Chang, Yu Chen, Zijun Chen, Ben Chiaro, Desmond Chik, Charina Chou, Jahan Claes, Agnetta Y. Cleland, Josh Cogan, Roberto Collins, Paul Conner, William Courtney, Alexander L. Crook, Ben Curtin, Sayan Das, Alex Davies, Laura De Lorenzo, Dripto M. Debroy, Sean Demura, Michel Devoret, Agustin Di Paolo, Paul Donohoe, Ilya Drozdov, Andrew Dunsworth, Clint Earle, Thomas Edlich, Alec Eickbusch, Aviv Moshe Elbag, Mahmoud Elzouka, Catherine Erickson, Lara Faoro, Edward Farhi, Vinicius S. Ferreira, Leslie Flores Burgos, Ebrahim Forati, Austin G. Fowler, Brooks Foxen, Suhas Ganjam, Gonzalo Garcia, Robert Gasca, Élie Genois, William Giang, Craig Gidney, Dar Gilboa, Raja Gosula, Alejandro Grajales Dau, Dietrich Graumann, Alex Greene, Jonathan A. Gross, Steve Habegger, John Hall, Michael C. Hamilton, Monica Hansen, Matthew P. Harrigan, Sean D. Harrington, Francisco J. H. Heras, Stephen Heslin, Paula Heu, Oscar Higgott, Gordon Hill, Jeremy Hilton, George Holland, Sabrina Hong, Hsin-Yuan Huang, Ashley Huff, William J. Huggins, Lev B. Ioffe, Sergei V. Isakov, Justin Iveland, Evan Jeffrey, Zhang Jiang, Cody Jones, Stephen Jordan, Chaitali Joshi, Pavol Juhas, Dvir Kafri, Hui Kang, Amir H. Karamlou, Kostyantyn Kechedzhi, Julian Kelly, Trupti Khaire, Tanuj Khattar, Mostafa Khezri, Seon Kim, Paul V. Klimov, Andrey R. Klots, Bryce Kobrin, Pushmeet Kohli, Alexander N. Korotkov, Fedor Kostritsa, Robin Kothari, Borislav Kozlovskii, John Mark Kreikebaum, Vladislav D. Kurilovich, Nathan Lacroix, David Landhuis, Tiano Lange-Dei, Brandon W. Langley, Pavel Laptev, Kim-Ming Lau, Loïck Le Guevel, Justin Ledford, Joonho Lee, Kenny Lee, Yuri D. Lensky, Shannon Leon, Brian J. Lester, Wing Yan Li, Yin Li, Alexander T. Lill, Wayne Liu, William P. Livingston, Aditya Locharla, Erik Lucero, Daniel Lundahl, Aaron Lunt, Sid Madhuk, Fionn D. Malone, Ashley Maloney, Salvatore Mandrà, James Manyika, Leigh S. Martin, Orion Martin, Steven Martin, Cameron Maxfield, Jarrod R. McClean, Matt McEwen, Seneca Meeks, Anthony Megrant, Xiao Mi, Kevin C. Miao, Amanda Mieszala, Reza Molavi, Sebastian Molina, Shirin Montazeri, Alexis Morvan, Ramis Movassagh, Wojciech Mruczkiewicz, Ofer Naaman, Matthew Neeley, Charles

Neill, Ani Nersisyan, Hartmut Neven, Michael Newman, Jiun How Ng, Anthony Nguyen, Murray Nguyen, Chia-Hung Ni, Murphy Yuezhen Niu, Thomas E. O'Brien, William D. Oliver, Alex Opremcak, Kristoffer Ottosson, Andre Petukhov, Alex Pizzuto, John Platt, Rebecca Potter, Orion Pritchard, Leonid P. Pryadko, Chris Quintana, Ganesh Ramachandran, Matthew J. Reagor, John Redding, David M. Rhodes, Gabrielle Roberts, Eliott Rosenberg, Emma Rosenfeld, Pedram Roushan, Nicholas C. Rubin, Negar Saei, Daniel Sank, Kannan Sankaragomathi, Kevin J. Satzinger, Henry F. Schurkus, Christopher Schuster, Andrew W. Senior, Michael J. Shearn, Aaron Shorter, Noah Shutty, Vladimir Shvarts, Shraddha Singh, Volodymyr Sivak, Jindra Skruzny, Spencer Small, Vadim Smelyanskiy, W. Clarke Smith, Rolando D. Somma, Sofia Springer, George Sterling, Doug Strain, Jordan Suchard, Aaron Szasz, Alex Sztein, Douglas Thor, Alfredo Torres, M. Mert Torunbalci, Abeer Vaishnav, Justin Vargas, Sergey Vdovichev, Guifre Vidal, Benjamin Villalonga, Catherine Vollgraff Heidweiller, Steven Waltman, Shannon X. Wang, Brayden Ware, Kate Weber, Travis Weidel, Theodore White, Kristi Wong, Bryan W. K. Woo, Cheng Xing, Z. Jamie Yao, Ping Yeh, Bicheng Ying, Juhwan Yoo, Noureldin Yosri, Grayson Young, Adam Zalcman, Yaxing Zhang, Ningfeng Zhu and Nicholas Zobrist, Quantum error correction below the surface code threshold, Nature 638, 920-926 (2025).

- [12] M. AbuGhanem, Google Quantum AI's Quest for Error-Corrected Quantum Computers, arXiv preprint arXiv:2410.00917 (2024).
- [13] Mario Motta, Gavin O. Jones, Julia E. Rice, Tanvi P. Gujarati, Rei Sakuma, Ieva Liepuoniute, Jeannette M. Garciaa and Yu-ya Ohnishi, Quantum chemistry simulation of ground- and excited-state properties of the sulfonium cation on a superconducting quantum processor, Chem. Sci. 14, 2915-2927 (2023).
- [14] Nick S. Blunt, Joan Camps, Ophelia Crawford, Róbert Izsák, Sebastian Leontica, Arjun Mirani, Alexandra E. Moylett, Sam A. Scivier, Christoph Sünderhauf, Patrick Schopf, Jacob M. Taylor, Nicole Holzmann, Perspective on the Current State-of-the-Art of Quantum Computing for Drug Discovery Applications, J. Chem. Theory Comput. 18, 12, 7001–7023 (2022).
- [15] Raffaele Santagati, Alan Aspuru-Guzik, Ryan Babbush, Matthias Degroote, Leticia González, Elica Kyoseva, Nikolaj Moll, Markus Oppel, Robert M. Parrish, Nicholas C. Rubin, Michael Streif, Christofer S. Tautermann, Horst Weiss, Nathan Wiebe and Clemens Utschig-Utschig, Drug design on quantum computers, Nature Physics 20, 549–557 (2024).
- [16] Frank Phillipson. Quantum computing in logistics and supply chain management an overview. arXiv:2402.17520, (2024).
- [17] P. W. Shor, Polynomial-time algorithms for prime factorization and discrete logarithms on a quantum computer. SIAM J. Comput. 26, 1484–1509 (1997).
- [18] Craig Gidney and Martin Ekerå, How to factor 2048 bit RSA integers in 8 hours using 20 million noisy qubits, Quantum 5, 433 (2021).
- [19] M. AbuGhanem, "Photonic Quantum Computers," arXiv:2409.08229, (2024).
- [20] A. Y. Kitaev. Fault-tolerant quantum computation by anyons. Annals of Physics 303(1), 2–30. (2003).

- [21] P. W. Shor, Fault-tolerant quantum computation. Proceedings of the 37th Annual Symposium on Foundations of Computer Science, Burlington, VT, USA (pp. 56–65). IEEE. (1996).
- [22] John Preskill, Quantum Computing in the NISQ era and beyond, Quantum 2, 79 (2018).
- [23] Michael E. Beverland, Prakash Murali, Matthias Troyer, Krysta M. Svore, Torsten Hoefler, Vadym Kliuchnikov, Guang Hao Low, Mathias Soeken, Aarthi Sundaram, Alexander Vaschillo, Assessing requirements to scale to practical quantum advantage, arXiv:2211.07629 (2022).
- [24] T. Toffoli, Reversible computing, In: de Bakker, J., van Leeuwen, J. (eds) Automata, Languages and Programming. ICALP 1980. Lecture Notes in Computer Science, vol 85. Springer, Berlin, Heidelberg. (1980).
- [25] M. A. Nielsen and I. L. Chuang, Quantum computation and quantum information, Cambridge: Cambridge University Press, 10th anniversary ed., (2011).
- [26] Fedorov, A., Steffen, L., Baur, M., et al. Implementation of a Toffoli gate with superconducting circuits. Nature 481(7380), 170–172. (2012).
- [27] M. AbuGhanem, Superconducting quantum computers: who is leading the future?. EPJ Quantum Technology 12, 102 (2025).
- [28] Barenco, A., Bennett, C. H., Cleve, R., et al. Elementary gates for quantum computation. Physical Review A 52(5), 3457–3467 (1995).
- [29] V. V. Shende, S. S. Bullock and I. L. Markov, "Synthesis of quantum-logic circuits," in *IEEE Transactions on Computer-Aided Design of Integrated Circuits and Systems*, vol. 25, no. 6, pp. 1000-1010, (2006).
- [30] Abhinav Kandala, Kristan Temme, Antonio D. Córcoles, Antonio Mezzacapo, Jerry M. Chow, Jay M. Gambetta, Error mitigation extends the computational reach of a noisy quantum processor, *Nature* 567, 491–495 (2019).
- [31] M. Amy, D. Maslov, M. Mosca and M. Roetteler, A meet-in-the-middle algorithm for fast synthesis of depth-optimal quantum circuits. IEEE Transactions on Computer-Aided Design, 32(6), 818-830. (2013).
- [32] S. T. Merkel, J. M. Gambetta, J. A. Smolin, S. Poletto, A. D. Corcoles, B. R. Johnson, C. A. Ryan, and M. Steffen, "Self-consistent quantum process tomography," *Phys. Rev. A* 87, 062119 (2013).
- [33] I. L. Chuang and M. A. Nielsen, "Prescription for experimental determination of the dynamics of a quantum black box," J. Mod. Opt. 44, 2455 (1997).
- [34] J. F. Poyatos, J. I. Cirac, and P. Zoller, "Complete characterization of a quantum process: the two-bit quantum gate," *Phys. Rev. Lett.* 78, 390 (1997).
- [35] M. AbuGhanem and H. Eleuch, "Full quantum tomography study of Google's Sycamore gate on IBM's quantum computers," *EPJ Quantum Technology* **11**(1), 36 (2024).
- [36] M. AbuGhanem, "Experimental characterization of Google's Sycamore quantum AI on IBM's quantum computers," *Elsevier*, SSRN 4299338 (2025).
- [37] H. N. Tinkey et al. Quantum process tomography of a Mølmer–Sørensen gate via a global beam. Quantum Sci. Technol. 6, 034013 (2021).
- [38] M. AbuGhanem and H. Eleuch, "Two-qubit entangling gates for superconducting quantum computers," *Results* in *Physics* 56, 107236 (2024).

- [39] Kishor Bharti, Alba Cervera-Lierta, Thi Ha Kyaw, Tobias Haug, Sumner Alperin-Lea, Abhinav Anand, Matthias Degroote, Hermanni Heimonen, Jakob S. Kottmann, Tim Menke, Wai-Keong Mok, Sukin Sim, Leong-Chuan Kwek, Alán Aspuru-Guzik, Noisy intermediate-scale quantum algorithms, Rev. Mod. Phys. 94, (2022).
- [40] Chufan Lyu, Xusheng Xu, Man-Hong Yung, and Abolfazl Bayat. "Symmetry enhanced variational quantum spin eigensolver". Quantum 7, 899 (2023).
- [41] Sergey Bravyi, Alexander Kliesch, Robert Koenig, and Eugene Tang. "Obstacles to Variational Quantum Optimization from Symmetry Protection". *Physical Review Letters* 125, 260505 (2020).
- [42] Chufan Lyu, Victor Montenegro, and Abolfazl Bayat. "Accelerated variational algorithms for digital quantum simulation of many-body ground states". Quantum 4, 324 (2020).
- [43] Panagiotis Kl Barkoutsos, Jerome F. Gonthier, Igor Sokolov, Nikolaj Moll, Gian Salis, Andreas Fuhrer, Marc Ganzhorn, Daniel J. Egger, Matthias Troyer, Antonio Mezzacapo, Stefan Filipp, and Ivano Tavernelli. "Quantum algorithms for electronic structure calculations: Particle-hole Hamiltonian and optimized wave-function expansions". Physical Review A 98, 022322 (2018).
- [44] Hanrui Wang, Yongshan Ding, Jiaqi Gu, Yujun Lin, David Z. Pan, Frederic T. Chong, and Song Han. "QuantumNAS: Noise-Adaptive Search for Robust Quantum Circuits". Proceedings - International Symposium on High-Performance Computer Architecture 2022-April, 692–708 (2021).
- [45] Yuxuan Du, Tao Huang, Shan You, Min Hsiu Hsieh, and Dacheng Tao. "Quantum circuit architecture search for variational quantum algorithms". npj Quantum Information 8, 62 (2022).
- [46] Yuhan Huang, Qingyu Li, Xiaokai Hou, Rebing Wu, Man-Hong Yung, Abolfazl Bayat, and Xiaoting Wang. "Robust resource-efficient quantum variational ansatz through evolutionary algorithm". *Physical Review A* 105, 052414 (2022).
- [47] Lukasz Cincio, Kenneth Rudinger, Mohan Sarovar, and Patrick J. Coles. "Machine Learning of Noise-Resilient Quantum Circuits". PRX Quantum 2, 010324 (2021).
- [48] Sophia Fuhui Lin, Sara Sussman, Casey Duckering, Pranav S Mundada, Jonathan M Baker, Rohan S Kumar, Andrew A Houck, and Frederic T Chong. "Let Each Quantum Bit Choose Its Basis Gates" arXiv:2208.13380. (2022).
- [49] Nikita A. Nemkov, Evgeniy O. Kiktenko, Ilia A. Luchnikov, and Aleksey K. Fedorov, Efficient variational synthesis of quantum circuits with coherent multi-start optimization, Quantum 7, 993 (2023).
- [50] Harsha Nagarajan, Owen Lockwood, and Carleton Coffrin. "QuantumCircuitOpt: An Open-source Framework for Provably Optimal Quantum Circuit Design". Proceedings of QCS 2021: 2nd International Workshop on Quantum Computing Software, Held in conjunction with SC 2021: The International Conference for High Performance Computing, Networking, Storage and Analysis Pages 55–63 (2021).
- [51] Matthew Amy, Dmitri Maslov, Michele Mosca, and Martin Roetteler. "A Meet-in-the-Middle Algorithm for Fast Synthesis of DepthOptimal Quantum Circuits". IEEE Transactions on Computer-Aided Design of In-

- tegrated Circuits and Systems 32, 818-830 (2013).
- [52] Sumeet Khatri, Ryan LaRose, Alexander Poremba, Lukasz Cincio, Andrew T. Sornborger, and Patrick J. Coles. "Quantum-assisted quantum compiling". Quantum 3 (2019).
- [53] Yunseong Nam, Neil J. Ross, Yuan Su, Andrew M. Childs, and Dmitri Maslov. "Automated optimization of large quantum circuits with continuous parameters". npj Quantum Information 4 (2018).
- [54] Richard Meister, Cica Gustiani, and Simon C. Benjamin. "Exploring ab initio machine synthesis of quantum circuits" arXiv:2206.11245. (2022).
- [55] Ethan Smith, Marc Grau Davis, Jeffrey Larson, E D Younis, Lindsay Bassman Oftelie, Wim Lavrijsen, Costin Iancu, Marc Grau Davis, Ed Younis, Bassman Lindsay, Wim Oftelie, and Costin Lavrijsen. "LEAP: Scaling Numerical Optimization Based Synthesis Using an Incremental Approach". ACM Transactions on Quantum Computing 4, 1–23 (2023).
- [56] Ho Lun Tang, V. O. Shkolnikov, George S. Barron, Harper R. Grimsley, Nicholas J. Mayhall, Edwin Barnes, and Sophia E. Economou. "Qubit-ADAPT-VQE: An Adaptive Algorithm for Constructing Hardware-Efficient Ansätze on a Quantum Processor". PRX Quantum 2, 1–15 (2021).
- [57] Harper R. Grimsley, Sophia E. Economou, Edwin Barnes, and Nicholas J. Mayhall. "An adaptive variational algorithm for exact molecular simulations on a quantum computer". *Nature Communications* 2019 10:1 10, 1–9 (2019).
- [58] Lukas Franken, Bogdan Georgiev, Sascha Mücke, Moritz Wolter, Raoul Heese, Christian Bauckhage, and Nico Piatkowski. "Quantum Circuit Evolution on NISQ Devices" arXiv:2012.13453. (2020).
- [59] D. Chivilikhin, A. Samarin, V. Ulyantsev, I. Iorsh, A. R. Oganov, and O. Kyriienko. "MoG-VQE: Multiobjective genetic variational quantum eigensolver" arXiv:2007.04424. (2020).
- [60] Mathias Weiden, John Kubiatowicz, Ed Younis, and Costin Iancu. "Ansatz Learning for Quantum Circuit Optimization". Bulletin of the American Physical Society (2023).
- [61] Thomas Fösel, Murphy Yuezhen Niu, Florian Marquardt, and Li Li. "Quantum circuit optimization with deep reinforcement learning" arXiv:2103.07585. (2021).
- [62] Péter Rakyta and Zoltán Zimborás. "Efficient quantum gate decomposition via adaptive circuit compression" arXiv:2203.04426. (2022).
- [63] Ed Younis, Koushik Sen, Katherine Yelick, and Costin Iancu. "QFAST: Conflating Search and Numerical Optimization for Scalable Quantum Circuit Synthesis". Proceedings - 2021 IEEE International Conference on Quantum Computing and Engineering, QCE 2021 Pages 232-243 (2021).
- [64] Péter Rakyta and Zoltán Zimborás. "Approaching the theoretical limit in quantum gate decomposition" arXiv:2109.06770. (2021).
- [65] Liam Madden and Andrea Simonetto. "Best Approximate Quantum Compiling Problems". ACM Transactions on Quantum Computing 3, 1–29 (2021).
- [66] Bobak Toussi Kiani, Seth Lloyd, and Reevu Maity. "Learning Unitaries by Gradient Descent" arXiv:2001.11897. (2020)

- [67] A. W. Cross, A. Javadi-Abhari, T. Alexander, N. de Beaudrap, L. S. Bishop, S. Heidel, C. A. Ryan, J. Smolin, J. M. Gambetta, and B. R. Johnson, "OpenQASM 3: A broader and deeper quantum assembly language," arXiv:2104.14722, (2021).
- [68] G. S. Paraoanu, Microwave-induced coupling of superconducting qubits, Phys. Rev. B 74:140504 (2006).
- [69] M. Möttönen, J. J. Vartiainen, V. Bergholm, and M. M. Salomaa, "Quantum circuits for general multiqubit gates," *Physical Review Letters*, 93 13, 130502, (2004).
- [70] J. J. Vartiainen, M. Möttönen, and M. M. Salomaa, "Efficient decomposition of quantum gates," *Physical Review Letters*, 92, 17, 177902, (2004).
- [71] V. V. Shende, S. S. Bullock, and I. L. Markov, "Synthesis of quantum-logic circuits," *IEEE Transactions on Computer-Aided Design of Integrated Circuits and Systems*, 25 6, 1000–1010, (2006).
- [72] M. G. Davis, E. Smith, A. Tudor, K. Sen, I. Siddiqi, and C. Iancu, "Towards optimal topology aware quantum circuit synthesis," in *International Conference on Quantum Computing and Engineering*. IEEE, 223–234 (2020)
- [73] C. Jones, "Low-overhead constructions for the faulttolerant Toffoli gate," *Physical Review A*, 87 2, 022328, (2013).
- [74] R. Cleve and J. Watrous, "Fast parallel circuits for the quantum Fourier transform," in *Proceedings of the 41st Annual Symposium on Foundations of Computer Science*. *IEEE*, 526–536 (2000).
- [75] X. Cheng, Z. Guan, and W. Ding, "Mapping from multiple-control Toffoli circuits to linear nearest neighbor quantum circuits," *Quantum Information Process*ing, 17 7, 1–26, (2018).
- [76] S. Hu, D. Maslov, M. Pistoia, and J. Gambetta, "Efficient circuits for quantum search over 2D square lattice architecture," in *Proceedings of the 56th Annual Design Automation Conference*, 1–2, (2019).
- [77] Qiskit, https://www.ibm.com/quantum/qiskit. Accessed April (2025).
- [78] S. Sivarajah, S. Dilkes, A. Cowtan, W. Simmons, A. Edgington, and R. Duncan, "t|ket>: A retargetable compiler for NISQ devices," *Quantum Science and Technology*, 6 1, 014003, (2020).
- [79] Cirq developers, "Cirq," Available: https://zenodo. org/record/5182845, (2021). Accessed April 05, 2025.
- [80] D. Maslov, G. W. Dueck, D. M. Miller, and C. Negrevergne, "Quantum circuit simplification and level compaction," *IEEE Transactions on Computer-Aided Design of Integrated Circuits and Systems*, 27 3, 436–444, (2008).
- [81] B. Kraus and J. Cirac, "Optimal creation of entanglement using a two-qubit gate," *Physical Review A*, 63 6, 062309, (2001).
- [82] J. Liu, Li, and H. Zhou, "Not all swaps have the same cost: A case for optimization-aware qubit routing," in 2022 IEEE International Symposium on High-Performance Computer Architecture (HPCA). IEEE, 709–725, (2022).
- [83] J. Liu, L. Bello, and H. Zhou, "Relaxed peephole optimization: A novel compiler optimization for quantum circuits," in 2021 IEEE/ACM International Symposium on Code Generation and Optimization(CGO). IEEE, 301–314. (2021).

- [84] P. Murali, D. C. McKay, M. Martonosi, and A. Javadi-Abhari, "Software mitigation of crosstalk on noisy intermediate-scale quantum computers," in Proceedings of the Twenty-Fifth International Conference on Architectural Support for Programming Languages and Operating Systems, 1001–1016, (2020).
- [85] K. N. Smith, G. S. Ravi, Murali, J. M. Baker, N. Earnest, A. Javadi-Cabhari and F. T. Chong, "Timestitch: Exploiting slack to mitigate decoherence in quantum circuits," ACM Transactions on Quantum Computing, 4, 1, 1–27, (2022).
- [86] J. Liu, M. Bowman, Gokhale, S. Dangwal, J. Larson, F. T. Chong, and P. D. Hovland, "Qcontext: Contextaware decomposition for quantum gates," in 2023 IEEE International Symposium on Circuits and Systems (IS-CAS) pp. 1–5 (2023).
- [87] Y. Shi, Both toffoli and controlled-not need little help to do universal quantum computing, Quantum Info. Comput. 3, 84-92 (2003).
- [88] D. Aharonov, A simple proof that toffoli and hadamard are quantum universal, arXiv:quant-ph/0301040, (2003).
- [89] E. Fredkin and T. Toffoli, Conservative logic, Int. J. Theor. Phys. 21(3-4), 219-253 (1982).
- [90] M. AbuGhanem, "Characterizing Grover search algorithm on large-scale superconducting quantum computers," *Scientific Reports* **15** (1), 1281 (2024).
- [91] T. Häner, M. Roetteler, and K. M. Svore, Factoring using 2n+2 qubits with toffoli based modular multiplication, Quantum Info. Comput. 17, 673-684 (2017).
- [92] P. W. Shor, Polynomial-time algorithms for prime factorization and discrete logarithms on a quantum computer, SIAM J. Comput. 26(5), 1484–1509 (1997).
- [93] A. Paetznick and B. W. Reichardt, Universal faulttolerant quantum computation with only transversal gates and error correction, *Phys. Rev. Lett.* 111(9), 090505 (2013).
- [94] E. Dennis, Toward fault-tolerant quantum computation without concatenation, Phys. Rev. A 63(5), 052314 (2001)
- [95] P. Schindler, J. T. Barreiro, and T. Monz et al., Experimental repetitive quantum error correction, Science 332(6033), 1059–1061 (2011).
- [96] D. G. Cory, M. D. Price, and W. Maas et al., Experimental quantum error correction, Phys. Rev. Lett. 81(10), 2152–2155 (1998).
- [97] M. D. Reed, L. DiCarlo, and S. E. Nigg et al., Realization of three-qubit quantum error correction with super-conducting circuits, Nature 482(7385), 382–385 (2012).
- [98] N. Yu, R. Duan, and M. Ying, Five 2-qubit gates are necessary for implementing the Toffoli gate, *Phys. Rev.* A 88(1), 010304 (2013).
- [99] V. V. Shende and I. L. Markov, On the CNOT-cost of TOFFOLI gates, arXiv:0803.2316 (2009).
- [100] J. Gwinner, M. Briański, W. Burkot, L. Czerwiński, and V. Hlembotskyi, Benchmarking 16-element quantum search algorithms on superconducting quantum processors, arXiv:2007.06539 (2021).
- [101] Takahiko Satoh, Shun Oomura, Michihiko Sugawara, and Naoki Yamamoto. Pulse-engineered controlled-V gate and its applications on superconducting quantum device. *IEEE Transactions on Quantum Engineering*, 3 (2022)

- [102] Max Aksel Bowman, Pranav Gokhale, Jeffrey Larson, Ji Liu, Martin Suchara, Hardware-Conscious Optimization of the Quantum Toffoli Gate, ACM Transactions on Quantum Computing 4, 4, 1-19, (2023).
- [103] Pedro M. Q. Cruz, Bruno Murta, Shallow unitary decompositions of quantum Fredkin and Toffoli gates for connectivity-aware equivalent circuit averaging, APL Quantum 1, 016105 (2024).
- [104] Xiangyu Ren, Mengyu Zhang, Antonio Barbalace, A Hardware-Aware Gate Cutting Framework for Practical Quantum Circuit Knitting, arXiv:2409.03870 (2024).
- [105] Ahmad Bennakhi, Gregory T. Byrd, Paul Franzon, Analyzing Quantum Circuit Depth Reduction with Ancilla Qubits in MCX Gates, arXiv:2408.01304 (2024).
- [106] Yun-Jie Wang, Sheng Zhang, Tai-Ping Sun, Ze-An Zhao, Xiao-Fan Xu, Xi-Ning Zhuang, Huan-Yu Liu, Cheng Xue, Peng Duan, Yu-Chun Wu, Zhao-Yun Chen,3, and Guo-Ping Guo, Hardware-Efficient Quantum Random Access Memory Design with a Native Gate Set on Superconducting Platforms, arXiv:2306.10250 (2024).
- [107] C. Duckering, J. M. Baker, A. Litteken, and F. T. Chong, "Orchestrated Trios: Compiling for Efficient Communication in Quantum Programs with 3-Qubit Gates," in Proceedings of the 26th ACM International Conference on Architectural Support for Programming Languages and Operating Systems, ASPLOS '21 (Association for Computing Machinery, New York, NY, USA, 2021) p. 375–385 (2021).
- [108] M. AbuGhanem, Hardware-aware Toffoli gate decomposition via echoed cross-resonance gates. Quantum Stud.: Math. Found. 12, 24 (2025).
- [109] D. L. Underwood, J. A. Glick, K. Inoue, D. J. Frank, J. Timmerwilke, E. Pritchett, S. Chakraborty, K. Tien, M. Yeck, J. F. Bulzacchelli, C. Baks, Rosno, R. Robertazzi, M. Beck, R. V. Joshi, D. Wisnieff, D. Ramirez, J. Ruedinger, S. Lekuch, B. P. Gaucher, D. J. Friedman Using cryogenic CMOS control electronics to enable a 2-qubit cross-resonance gate, arXiv:2302.11538, (2023).
- [110] P. Jurcevic, A. Javadi-Abhari, L. S. Bishop, I. Lauer, D. F. Bogorin, M. Brink, L. Capelluto, O. Günlük, T. Itoko, N. Kanazawa, A. Kandala, G. A. Keefe, K. Krsulich, W. Landers, E. P. Lewandowski, D. T. McClure, G. Nannicini, A. Narasgond, H. M. Nayfeh, E. Pritchett, M. B. Rothwell, S. Srinivasan, N. Sundaresan, C. Wang, K. X. Wei, C. J. Wood, J.-B. Yau, E. J. Zhang, O. E. Dial, J. M. Chow, and J. M. Gambetta, Demonstration of quantum volume 64 on a superconducting quantum computing system, Quantum Science and Technology, 6, 2, 025020 (2021).
- [111] N. Sundaresan, I. Lauer, E. Pritchett, E. Magesan, Jurcevic, and J. M. Gambetta, Reducing Unitary and Spectator Errors in Cross Resonance with Optimized Rotary Echoes, PRX Quantum, 1, 2, 020318 (2020).
- [112] S. Sheldon, E. Magesan and J. Chow, J. Gambetta, Procedure for systematically tuning up cross-talk in

- the cross-resonance gate. Phys. Rev. A $\bf 93$, 060302(R). (2016).
- [113] José D. Guimarães, James Lim, Mikhail I. Vasilevskiy, Susana F. Huelga, Martin B. Plenio, Noise-assisted digital quantum simulation of open systems, *PRX Quantum* 4, 040329 (2023).
- [114] J. A. Smolin, J. M. Gambetta and G. Smith. Efficient method for computing the maximum-likelihood quantum state from measurements with additive Gaussian noise. *Phys. Rev. Lett.* 108, 070502, (2012).
- [115] Y. S. Teo et al. Quantum-state reconstruction by maximizing likelihood and entropy. Phys. Rev. Lett. 107, 020404, (2011).
- [116] D. F. James, P. G. Kwiat, W. J. Munro, and A. G. White. On the measurement of qubits. *Physical Review A* 64, 052312 (2001).
- [117] E. Bolduc, G. C. Knee, E. M. Gauger, and J. Leach. Projected gradient descent algorithms for quantum state tomography. npj Quantum Information 3 (2017).
- [118] B. Qi et al. Adaptive quantum state tomography via linear regression estimation: Theory and two-qubit experiment. npj Quantum Information3 (2017).
- [119] Violeta N. Ivanova-Rohling, Niklas Rohling, Guido Burkard, Optimal quantum state tomography with noisy gates, EPJ Quantum Technology 10, 25 (2023).
- [120] R. C. Bialczak et al. Quantum process tomography of a universal entangling gate implemented with Josephson phase qubits. Nat. Phys. 6, 409–413 (2010).
- [121] R. Jozsa, Fidelity for mixed quantum states. J. Mod. Opt. 41(12), 2315–2323 (1994).
- [122] M. D. Choi. Completely positive linear maps on complex matrices. *Linear Algebra Appl.* 10, 285 (1975).
- [123] M. AbuGhanem et al. "Fast universal entangling gate for superconducting quantum computers," Elsevier, SSRN, 4726035 (2024).
- [124] K. Kraus. States, Effects, and Operations. Springer-Verlag. Berlin. (1983).
- [125] M.W. Mitchell et al. Diagnosis, prescription, and prognosis of a Bell-State filter by quantum process tomography Phys. Rev. Lett. 91, 120402 (2003).
- [126] J. L. O'Brien et al. Quantum process tomography of a controlled-not gate. Phys. Rev. Lett. 93, 080502 (2004).
- [127] A. Jamiołkowski. Linear transformations which preserve trace and positive semidefiniteness of operators. Rep. Math. Phys. 3, 275 (1972).
- [128] M. AbuGhanem, Full Quantum Process Tomography of a Universal Entangling Gate on an IBM's Quantum Computer. Arab J Sci Eng (2025).
- [129] M. Horodecki, P. Horodecki, and R. Horodecki, General teleportation channel, singlet fraction, and quasidistillation, *Phys. Rev. A* 60, 1888 (1999).
- [130] M. A. Nielsen, A simple formula for the average gate fidelity of a quantum dynamical operation, *Physics Let*ters A 303, 249 (2002).